NUREG/CR-6458

Moisture Characteristic Curves for Apache Leap Tuff: Temperature Effects and Hysteresis

Prepared by
C. R. Rhodes, L. G. Wilson, T. C. Rasmussen, R. L. Bassett

Edited by
C. Thies

The University of Arizona

Prepared for
U.S. Nuclear Regulatory Commission

DF02
0/1

9612030275 960930
PDR NUREG
CR-6458 R PDR

AVAILABILITY NOTICE

Availability of Reference Materials Cited in NRC Publications

Most documents cited in NRC publications will be available from one of the following sources:

1. The NRC Public Document Room, 2120 L Street, NW., Lower Level, Washington, DC 20555-0001

2. The Superintendent of Documents, U.S. Government Printing Office, P. O. Box 37082, Washington, DC 20402-9328

3. The National Technical Information Service, Springfield, VA 22161-0002

Although the listing that follows represents the majority of documents cited in NRC publications, it is not intended to be exhaustive.

Referenced documents available for inspection and copying for a fee from the NRC Public Document Room include NRC correspondence and internal NRC memoranda; NRC bulletins, circulars, information notices, inspection and investigation notices; licensee event reports; vendor reports and correspondence; Commission papers; and applicant and licensee documents and correspondence.

The following documents in the NUREG series are available for purchase from the Government Printing Office: formal NRC staff and contractor reports, NRC-sponsored conference proceedings, international agreement reports, grantee reports, and NRC booklets and brochures. Also available are regulatory guides, NRC regulations in the *Code of Federal Regulations*, and *Nuclear Regulatory Commission Issuances*.

Documents available from the National Technical Information Service include NUREG-series reports and technical reports prepared by other Federal agencies and reports prepared by the Atomic Energy Commission, forerunner agency to the Nuclear Regulatory Commission.

Documents available from public and special technical libraries include all open literature items, such as books, journal articles, and transactions. *Federal Register* notices, Federal and State legislation, and congressional reports can usually be obtained from these libraries.

Documents such as theses, dissertations, foreign reports and translations, and non-NRC conference proceedings are available for purchase from the organization sponsoring the publication cited.

Single copies of NRC draft reports are available free, to the extent of supply, upon written request to the Office of Administration, Distribution and Mail Services Section, U.S. Nuclear Regulatory Commission, Washington, DC 20555-0001.

Copies of industry codes and standards used in a substantive manner in the NRC regulatory process are maintained at the NRC Library, Two White Flint North, 11545 Rockville Pike, Rockville, MD 20852-2738, for use by the public. Codes and standards are usually copyrighted and may be purchased from the originating organization or, if they are American National Standards, from the American National Standards Institute, 1430 Broadway, New York, NY 10018-3308.

DISCLAIMER NOTICE

This report was prepared as an account of work sponsored by an agency of the United States Government. Neither the United States Government nor any agency thereof, nor any of their employees, makes any warranty, expressed or implied, or assumes any legal liability or responsibility for any third party's use, or the results of such use, of any information, apparatus, product, or process disclosed in this report, or represents that its use by such third party would not infringe privately owned rights.

NUREG/CR-6458

Moisture Characteristic Curves for Apache Leap Tuff: Temperature Effects and Hysteresis

Manuscript Completed: June 1996
Date Published: September 1996

Prepared by
C. R. Rhodes, L. G. Wilson, T. C. Rasmussen, R. L. Bassett

Edited by
C. Thies

Department of Hydrology and Water Resources
The University of Arizona
Tucson, AZ 85721

T. Nicholson, NRC Project Manager

Prepared for
Division of Regulatory Applications
Office of Nuclear Regulatory Research
U.S. Nuclear Regulatory Commission
Washington, DC 20555-0001
NRC Job Code L1282

ABSTRACT

Laboratory methods were used to define matrix hydraulic properties for low-permeability Apache Leap Tuff core segments. Moisture content/matric potential relationships, including hysteresis, and measured hydraulic conductivity data were determined at a constant laboratory temperature of 20° C. To investigate the effects of temperature on those relationships, additional retention data were obtained at 5° C and 45° C. Measured retention data at all temperatures were applied to the van Genuchten model RETC, which performs curve-fitting and calculation of the flow parameter hydraulic conductivity. Although data at 5° C proved to be inconclusive, increasing the temperature from 20 to 45° C produced a shift of the moisture characteristic curve toward a higher potential for a given water saturation. Model-calculated hydraulic conductivity also increased as temperature increased, with respect to water saturation. The temperature-dependent change in the viscosity of water proved inadequate to explain the increases of hydraulic conductivity with temperature.

TABLE OF CONTENTS

LIST OF FIGURES

LIST OF TABLES

ACKNOWLEDGEMENTS

This report has been prepared to document work performed to date by researchers in the Department of Hydrology and Water Resources at The University of Arizona, under contract NRC-04-90-51, FIN L1282, entitled "Validation Studies for Assessing Unsaturated Flow and Transport Through Fractured Rock." The project manager is Thomas J. Nicholson who provided substantial input to the preparation of this report. The report is an independent product and does not necessarily reflect the views or regulatory position of the NRC.

FOREWORD

This technical report was prepared by The University of Arizona under their research project with the Waste Management Branch in the Office of Nuclear Regulatory Research (FIN L1282). The focus of this research study was to evaluate site characterization methods for unsaturated, fractured rock. The report provides information on laboratory methods used for estimating moisture characteristic curves for unsaturated rock samples. Detailed information is provided on partially-saturated flow theories and models, methods and materials used in the laboratory evaluations, and experimental results which are all used in estimating moisture contents, hydraulic conductivities and vapor pressures of partially saturated, heterogeneous, fractured rock core specimens. Data summaries are also provided in the appendices. The research reported provides insights into uncertainties in the laboratory test results such as those due to temperature effects and hysteresis. The lessons learned are relevant to site characterization and data analysis issues for modeling unsaturated flow and transport in fractured rock.

NUREG/CR-6458 is not a substitute for NRC regulations, and compliance is not required. The approaches and/or methods described in this NUREG/CR are provided for information only. Publication of this report does not necessarily constitute NRC approval or agreement with the information contained herein. Use of product or trade names is for identification purposes only and does not constitute endorsement by the NRC or The University of Arizona.

1. INTRODUCTION

Large volumes of radioactive material are being produced on a daily basis in this country by industry and the government, including wastes from facilities for nuclear-generated power and government war surplus. This waste is currently in temporary storage, but preparations are being made for permanent underground disposal. The location under consideration as a permanent repository for high-level nuclear waste (HLNW) is Yucca Mountain, near the boundary of the Nevada Test Site in southern Nevada. The repository is designed to lie in unsaturated fractured volcanic rock, well above the regional water table.

The flow of liquid water in unsaturated fractured rock is expected to be a principal mechanism for the transport of radioactive contaminants from the proposed site to the accessible environment. Fluid flow behavior is a function, most importantly, of the properties of the geologic medium and the physical effects imposed on that environment by the emplaced repository. One of those effects will be extensive fracturing in the immediate vicinity of the repository. That problem will not be addressed here. Another important effect will be the large quantity of heat released at the site by the radioactive decay of nuclear waste. The decomposition process will create high temperatures, for which rock has only a limited capacity for conductance (Wang et al., 1981). The large amounts of generated heat could induce liquid-vapor countercurrent flow in the surrounding medium, where countercurrent describes the flow of water vapor away from a heat source, with a return flow of liquid toward the heat source (Matthews, 1986). Ignoring the effects of vapor flow, significant quantities of heat can produce substantial changes in hydraulic properties and, therefore, affect the transport of radioactive contaminants. Using granular porous media, workers from Philip and de Vries (1957) to Wilkinson and Klute (1962), Haridasan and Jensen (1972), and Hopmans and Dane (1985, 1986) found extensive evidence of temperature-induced increases in water potential and hydraulic conductivity with respect to water saturation.

Even without the complications of a thermally altered environment, accurate descriptions of unsaturated flow are difficult to obtain. It is necessary to determine the unsaturated hydraulic conductivity of each media type as a function of water content or matric potential. Measurement of unsaturated conductivity is a difficult and lengthy process, especially for low-permeability materials. For this reason, moisture retention data, which can be used to predict unsaturated hydraulic conductivity curves (van Genuchten, 1980), become critical to the hydrologic characterization of unsaturated porous media. Hysteretic and sorption data can also be useful for indicating the nature of the matric potential dependence on water content, knowledge which is crucial for predicting flow.

Comprehensive numerical models, like the model TOUGH, have been applied to multiphase transport problems in rock (Tsang and Pruess, 1987; Lindgren and Rasmuson, 1990). Such models use established theories of unsaturated flow of liquid, vapor, and heat in porous media. The models incorporate the influence of fluid pressure on fluid flow for both liquid and gaseous phases, the effects of viscous and gravity forces, and the influence of heat transport, where thermal conductivity is a function of the degree of saturation. The application of this type of model poses a much simpler problem when we first define hydraulic functions under isothermal conditions, than for problems requiring thermal gradients. Even under isothermal conditions, information on hydraulic functions as applied to rock is sparse. To that end, the objective of this research is two-fold: (a) to identify and examine the moisture content/matric potential relationships (i.e., moisture characteristic curves), including hysteresis, and the derived hydraulic conductivity relationship for low-permeability volcanic tuff at 20° C; and (b) to investigate the expected dependence of the

relationships of moisture retention and hydraulic conductivity on water content for a range of isothermal conditions.

In an effort to characterize the hydraulic properties of unsaturated volcanic tuff, a field site was selected with tuff similar to that found at the proposed HLNW site at Yucca Mountain. The Apache Leap Tuff Site, located near Superior, Arizona, has been the focus of field and laboratory studies to identify the mechanisms of flow in unsaturated fractured tuff (see Figure 1.1). Five blocks of partially welded tuff were removed from the site. One of these was labeled, cored, and subsequently used to perform the procedures described in this paper.

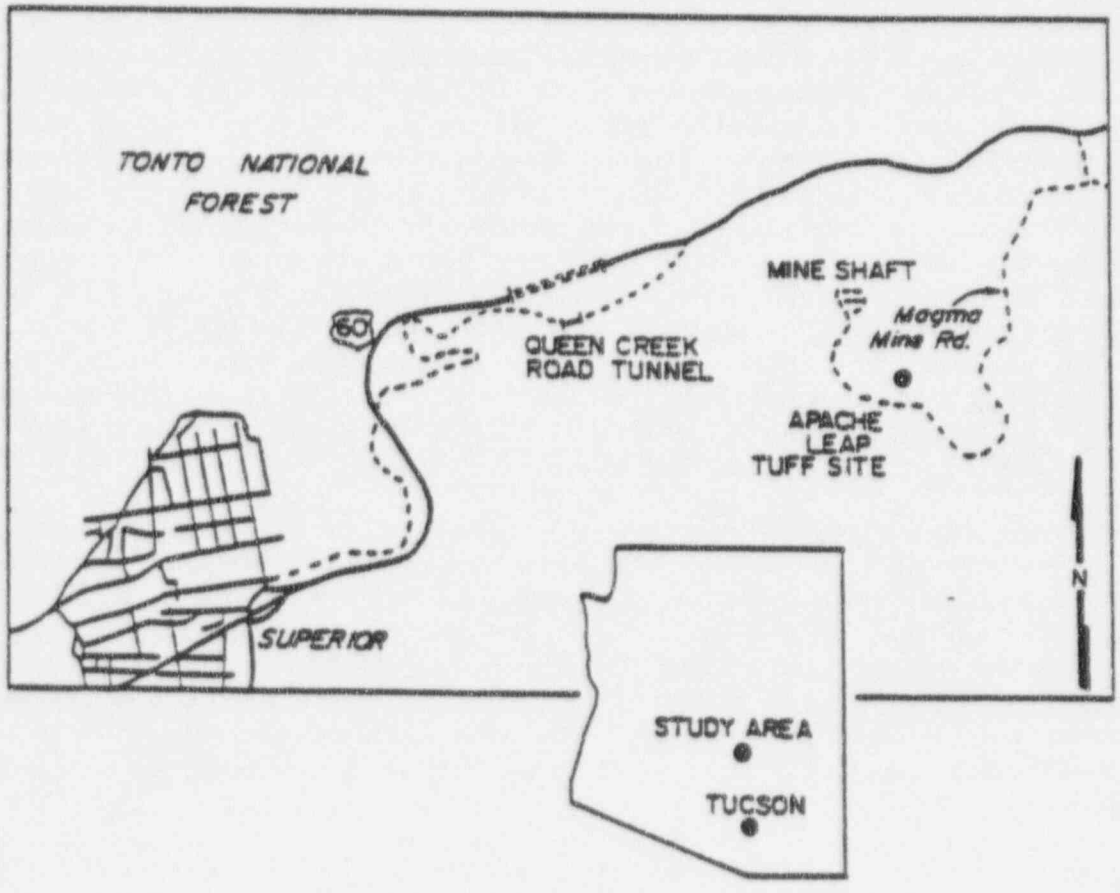

Figure 1.1 Location of the Apache Leap Tuff Site study area in Arizona.

2. THEORY

Water flow in partially saturated geologic media is described in one dimension using Richards equation (1931) as:

$$C(h)\frac{\partial h}{\partial t} = \frac{\partial}{\partial z}\left[K(h)\frac{\partial h}{\partial z} + K(h)\right] \tag{2.1}$$

where C(h) is the soil water capacity [m^{-1}], h is the pore water pressure head [m], t is time [s], z is vertical length [m], and K(h) is the hydraulic conductivity [m/s]. Soil water capacity can be estimated from the slope of the moisture characteristic curve, in which water content is a function of capillary pressure head. Given a homogeneous and unsaturated medium, Equation (2.1) may be written in terms of water content as:

$$\frac{\partial \theta}{\partial t} = \frac{\partial}{\partial z}\left[D(\theta)\frac{\partial \theta}{\partial z} + K(\theta)\right] \tag{2.2}$$

where θ is volumetric water content [m/m], and $D(\theta)$ is the soil water diffusivity [m^2/s] defined as:

$$D(\theta) = K(\theta)\frac{dh}{d\theta}. \tag{2.3}$$

While the moisture retention relationship, $\theta(h)$, can be measured with relative ease, the unsaturated hydraulic functions of hydraulic conductivity, as K(h) or $K(\theta)$, and pore water diffusivity $D(\theta)$ are more difficult to obtain. For that reason, several methods have been introduced to calculate these functions.

2.1 HYDRAULIC CONDUCTIVITY DETERMINATION

Burdine (1953) envisioned a porous medium as groups of parallel capillary tubes, with each group having a uniform pore size distribution and varying permeabilities. He introduced the importance of pore size distribution, with the concept that pores empty of fluids sequentially, beginning with the largest diameter pores. Previous models, as reviewed by Mualem (1986), had been used to derive relationships for effective saturation, S_e:

$$S_e = \frac{\theta - \theta_r}{\theta_s - \theta_r} \tag{2.4}$$

and relative hydraulic conductivity, K_r

$$K_r = \frac{K}{K_{sat}} = S_e^{\alpha} \tag{2.5}$$

where θ_s and θ_r represent the saturated and residual water contents, respectively. K_r proved to be a power function of effective saturation, where α is the fitting parameter. Burdine combined his

theory of pore size distribution with the relationships shown above into a new equation for unsaturated hydraulic conductivity, incorporating tortuousity as the exponent in the power function relationship with S_e, giving:

$$K_r(S_e) = S_e^2 \frac{\int_0^{S_e} \frac{1}{h^2(x)}\,dx}{\int_0^1 \frac{1}{h^2(x)}\,dx}. \qquad (2.6)$$

In order to minimize the frequent deviations found between measured $K(\theta)$ curves and those predicted from preceeding models, Mualem (1976a) proposed the following alternative to Burdine's model:

$$K_r = S_e \left[\frac{\int_0^{S_e} \frac{1}{h(x)}\,dx}{\int_0^1 \frac{1}{h(x)}\,dx} \right]^2 \qquad (2.7)$$

where l is a fitted pore-connectivity parameter with an estimated average of 0.5, based on measurements made by Mualem from many different soils. With the pore-connectivity parameter, l, Mualem's model takes into account pore length as well as cross-section, allowing larger pores to have a greater influence on K.

Brooks and Corey (1964) derived an empirical expression relating effective saturation to pressure head, taking the form:

$$h = \left[\alpha S_e^{\frac{1}{n}} \right]^{-1} \qquad (2.8)$$

describing an S-shaped curve where α and n are curve-fitting parameters to be determined from the experimental moisture retention data. Here, the parameter n was allowed to have any value greater than zero, taking a small value for media with broad pore-sized distribution and a large value for media with relatively uniform pore size.

A new S-shaped model for fitting retention data was proposed by van Genuchten (1980):

$$S_e = \left[1 + (\alpha h)^n \right]^{-m} \qquad (2.9)$$

where α, n, and m are, again, empirical curve-fitting parameters. The parameter n is related to matrix pore size distribution; the parameter m is a function of n; and the parameter α is inversely related to the air-entry value or bubbling pressure. By imposing some restrictions on the parameters m and n, and setting m=1-1/n, van Genuchten derived a closed-form solution for Mualem's Equation (2.7), resulting in the following expression:

$$K_r = S_e^l \left[1 - \left(1 - S_e^{\frac{1}{m}} \right)^m \right]^2 \tag{2.10}$$

where l is equal to 0.5. A similar form was derived from Burdine's model:

$$K_r = S_e^l \left[1 - \left(1 - S_e^{\frac{1}{m}} \right)^m \right] \tag{2.11}$$

for l = 2 and m = 1-2/n. In the analytical model RETC, van Genuchten et al. (1991) applied the Brooks and Corey model as well as van Genuchten's model to both Burdine's and Mualem's solutions for hydraulic conductivity. The several applications possible allowed for wide variation of the parameters m and n, by applying them as: (a) limited, with m(n), as in Equations (2.10) and (2.11); (b) the case for variable m and n; and (c) $n \rightarrow \infty$. It was found that application of the Burdine model is very limited for porous media with broad pore-size distributions (i.e., material for which $n \leq 2$), because K as given by Equation (2.11) will go to zero as n goes to two (van Genuchten and Nielsen, 1985). An important limitation of using variable m and n is that it often generates a value of $n < 1$, making the predictive equation for K invalid. For that reason, the case of variable m and n is recommended for use only with well-defined moisture retention data sets. After several experiments with the input variables, the van Genuchten solution to Mualem's model (Equation 2.10) and the variable m and n case were applied to the data from this study.

2.2 TEMPERATURE EFFECTS

Early research into the effects of temperature on the moisture-holding capacity of soils began late in the last century, with King in 1894 and Briggs in 1897, where surface tension and viscosity of water were soon recognized to be important mechanisms. In 1915, Bouyoucos postulated a strong link between temperature effects and entrapped air. Since then, researchers have attempted to quantify the effects of these mechanisms. The reader is referred to Nimmo (1983) for an excellent historical review of temperature-influenced surface tension and viscosity studies of granular porous media.

Philip and de Vries (1957) developed an expression for the effects of temperature on capillary pressure head due to changes in the surface tension of water:

$$\frac{\partial h}{\partial T} = \frac{h}{\sigma} \frac{d\sigma}{dT} = h\gamma \tag{2.12}$$

where $\partial h/\partial T$ is the temperature coefficient of pore water pressure head [m/° C], σ is the surface tension at the air-water interface [N/m], and γ is the temperature coefficient of surface tension of water [C^{-1}]. Experimental results published by Gardner (1955), Wilkinson and Klute (1962), and Hopmans and Dane (1985) indicated an increase in pressure head with increasing temperature for a given water content. Calculated results based on Equation (2.12), however, consistently underestimated the measured data by as much as several orders of magnitude. On the other hand, Haridasan and Jensen (1972) and Hopmans and Dane (1986) found little or no evidence of temperature effect when plotting hydraulic conductivity as a function of matric pressure. This

phenomenon was attributed to the counteracting effects of temperature on hydraulic conductivity and viscosity. Specifically, when temperature increases, hydraulic conductivity increases as the viscosity of water decreases; however, under transient conditions, hydraulic conductivity decreases as the water content at a given head decreases.

The inverse relationship of viscosity to unsaturated hydraulic conductivity is of primary importance in explaining the effects of temperature on that flow parameter. Hydraulic conductivity is defined as:

$$K = k \cdot \frac{\rho g}{\mu} \tag{2.13}$$

where k is the intrinsic permeability [m^2], ρ is liquid density [kg/m^3], g is gravity [m/s^2], and μ is the viscosity of the liquid [Pa·s]. The temperature coefficient of the density of liquid water, at 10^{-4} kg/l° C, is expected to have a negligible influence on matric hydraulic properties. Therefore, the effects of temperature on liquid density ρ are of essentially no consequence, and the effects of temperature on flow should be attributable to the inverse relationship of the change in viscosity μ with temperature. Constantz (1982) and Hopmans and Dane (1985, 1986) employed the viscosity ratio:

$$K_T = \frac{\mu_{ref}}{\mu_T} K_{ref} \tag{2.14}$$

where K_T is the hydraulic conductivity at the temperature of interest, K_{ref} is the hydraulic conductivity at the reference temperature, and μ_{ref} and μ_T represent viscosity of water at the reference temperature and the new water temperature, respectively. Haridasan and Jensen (1972) and Hopmans and Dane (1986), among others, observed temperature- induced increases in hydraulic conductivity at a given water content that could be accounted for almost entirely by the reduction in viscosity. On the other hand, Constantz (1982) and others (Nimmo, 1983) suggested there may be a greater temperature dependence of unsaturated hydraulic conductivity than that predicted solely by changes in water viscosity. For instance, it has been suggested that the temperature coefficient related to temperature-dependent viscosity may be greater for pore solution than for pure water. Constantz also suggests that the contribution of water vapor flux may be significant at higher temperatures. Because of the relative ease of, and greater success with, the application, it is the viscosity ratio method which will be used in this study to predict unsaturated hydraulic conductivity as a function of water content and temperature.

2.3 VAPOR PRESSURE DETERMINATION

According to Jackson (1964), the movement of water vapor in dry porous media is a complex process which incorporates vapor diffusion, evaporation and condensation, and adsorption of water molecules on solid surfaces. It is very difficult to quantify those various components of the vapor diffusion process. Instead, a basic relationship between water potential and vapor potential is applied to the problem of obtaining moisture contents at very low matric potentials.

The total potential of water, ψ_t in a pore water solution is the sum of the components gravity potential, ψ_g, matric potential, ψ_m, and osmotic potential, ψ_o, and can be expressed as:

$$\psi_t = gz + \frac{1}{\rho_w}(p - \Pi) \tag{2.15}$$

where g is gravity [N/kg], z is vertical length, ρ_w [kg/m$_3$] is density of pure water, p is matric pressure, and Π is the osmotic pressure [N/m^2] of the pore solution. Water is present, however, as both liquid and gas phases and, at static equilibrium, the total potentials of both phases are equal. Water vapor is not influenced by matric forces and, because it consists of pure water, the osmotic potential must equal zero. The total vapor potential, then, is subject only to vapor pressure and gravitational forces. By substituting ρ_{vap}, density of water vapor, for ρ_w into a form of the ideal gas law, one gets:

$$\rho_{vap} = \frac{pM}{RT}. \tag{2.16}$$

Substituting Equation (2.16) into the vapor potential form of Equation (2.15) yields a form which holds for isothermal conditions:

$$\psi_t(vap) = \int \frac{RT}{pM} dp + gz = \frac{RT}{M} \ln p + gz + C \tag{2.17}$$

where R is the molar gas constant [8.314 J/mol K], T is temperature in Kelvins, M is the molar mass of water [kg/mol], and C is an integration constant. At static equilibrium, gz is the same for liquid water as it is for water vapor at the gas-liquid interface, so that $\psi_t(liq) = \psi_t(vap) = gz$. Under these conditions, it follows:

$$C = -\frac{RT}{M}[\ln p_s] \tag{2.18}$$

where p_s is saturated vapor pressure (Koorevaar et al., 1983). One can substitute the expression for C into Equation (2.17) and set (2.17) equal to Equation (2.15), with results:

$$\frac{1}{\rho_w}(p - \Pi) = \frac{RT}{M} \ln \frac{p}{p_s} \tag{2.19}$$

where gz cancels from each side of the equation and p/p_s is the relative vapor pressure, also known as relative humidity. If a known vapor pressure is applied to the capillary environment, the total potential of the pore water should eventually equilibrate at the vapor pressure. From this relationship, the known vapor pressure/relative humidity of a saturated salt solution could be used to calculate an equivalent equilibrium pore pressure.

3. METHODS AND MATERIALS

The partially welded tuffaceous dacite used for the experiments was removed from beside the Magma Mine Road, approximately 91.5 meters before the turnoff to the Apache Leap Tuff site, shown in Figure 3.1 (Thompson, 1990). Maintaining vertical orientation, the block was cored, the cores were sliced, and the segment surfaces were ground smooth using water as the only coolant. Twenty samples were used to derive the moisture retention data. The samples measured six centimeters in diameter and range from 2.39 to 2.69 cm in height. Ten samples were used for one of the hysteresis loops, ranging from 2.61 to 2.79 cm in height. The core segments were labeled as to identification and orientation, measured to determine volume, and then placed in a drying oven at 105°C for 24 to 48 hours, depending on size and initial water content. Because the drying time was defined for soil samples, as recommended by Klute (1986), tuff samples were weighed periodically during oven drying to determine the necessary drying time. After cooling in a dessicator, the samples were sealed on the sides with heat shrink or adhesive-backed vinyl to prevent moisture losses through the sample sides. The prepared cores were then saturated under vacuum with de-aired 0.005 M $CaSO_4$ solution, as recommended by Klute (1986), and weighed again. The saturation setup is shown in Figure 3.2. The technique of vacuum-saturating samples with de-aired solution greatly reduced the occurrence of entrapped air. Porosity and volumetric water content were calculated using the relationship:

$$\theta = \frac{(m_w - m_d)}{\rho_l V}$$

where θ is volumetric water content [cm^3/cm^3], m_w is mass of the wet sample [g], m_d is mass of the dry sample [g], ρ_l is density of water at the temperature of interest [g cm^{-3}], and V is the volume of the sample [cm^3].

The core segments provided data for determining water content/matric potential relationships, including a wetting hysteresis scanning curve and a drying/wetting hysteresis loop. In addition, saturated hydraulic conductivity and intrinsic permeability were measured for some of the same samples. The wetter portions of the moisture characteristic curve were obtained by the use of computer-controlled pressure and a pressure extraction vessel (i.e., matric potentials from 0.01 to .5 MPa), while saturated salt solutions were used to obtain data for the drier regions (i.e., matric potentials less than .5 MPa). [Note that 0.1 MPa is equal to 100 kPa, is equal to 1 bar.] The wetting portions of the moisture characteristic curve were obtained by reversing the order of the applied pressure increments, with some modification to the extraction vessel setup. A complete set of desorption/absorption curves requires several months, depending on the permeability of the material being analyzed, the size of the samples, and the number of pressure steps employed, especially when vapor equilibration is required. Saturated hydraulic conductivity and intrinsic permeability were measured with a permeameter and a Tempe cell, respectively, also employing computer-controlled pressure.

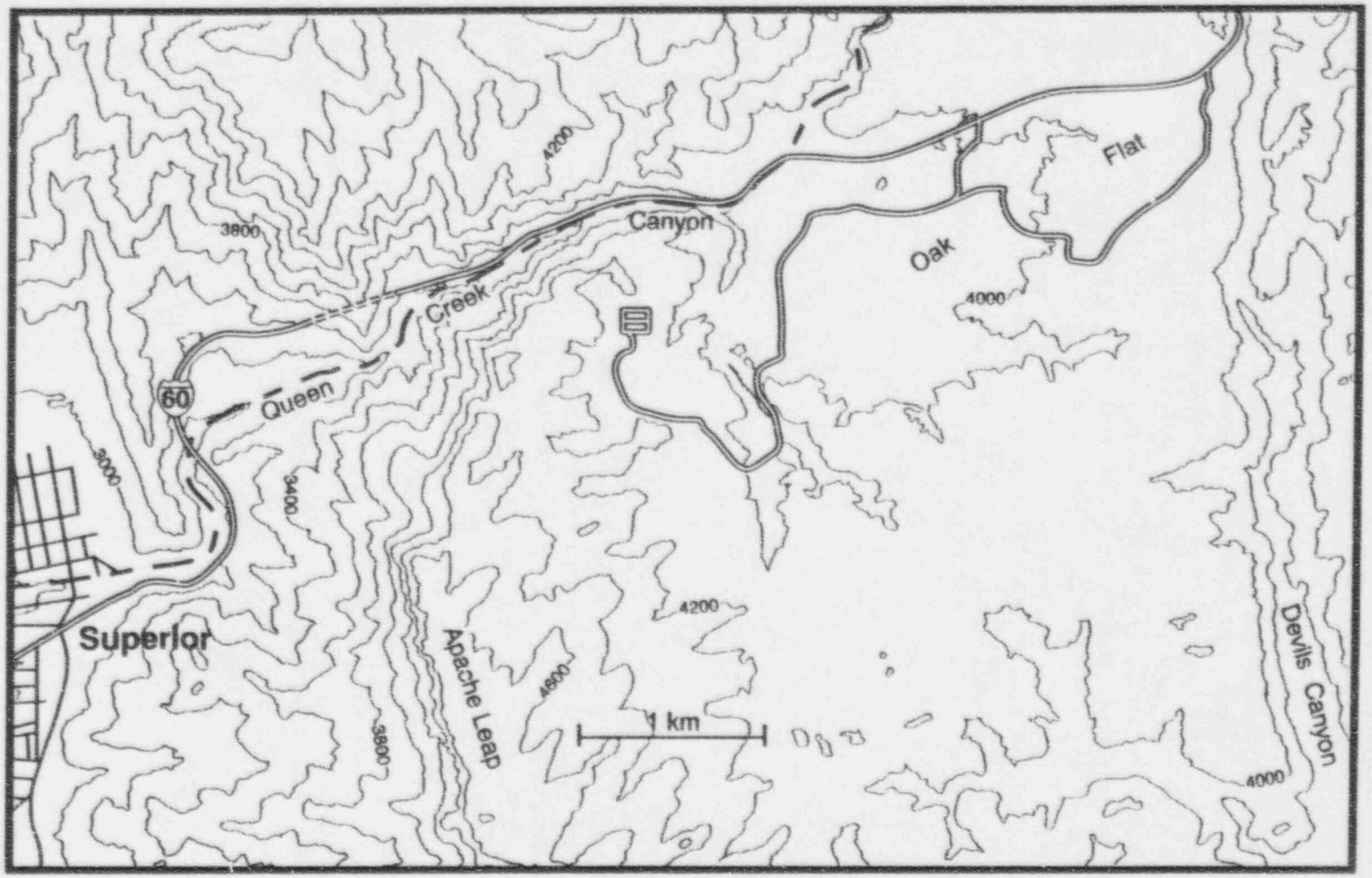

Figure 3.1 Contour map of Apache Leap Tuff Site (from U.S. Geological Survey map for Superior, Arizona, SE Superior 15' quadrangle, revised 1981).

3.1 PRESSURE PLATE EXTRACTOR METHOD

A pressure plate extractor was used to regulate the matric potential within tuff core segments for the wetter range. The pressure plate extraction technique has been employed for decades and is widely used to determine moisture retention relationships for soils (Richards, 1965). Recently, the method has also been applied with good results to consolidated samples such as sandstone (Rahi, 1986), basalt (Bishop, 1990), and volcanic tuff (Rahi, 1986; Flint, 1991). The basic method of equilibrating geologic samples under increasing increments of pressure, modified from a method suggested by Klute (1986), utilizes a computer monitored on-off solenoid, a pressure transducer, and a bleed-off solenoid to control pressure in the extraction vessel to within 2 kPa (Figure 3.3). The pressure transducer was a Setra Systems Model 205-2, with a range of 0-250 psi.

Effects of plate impedance on the capillary conductivity of granular porous media have been studied by Miller and Elrick (1958), Kunze and Kirkham (1962), and Valiantzas (1990). Information from the manufacturer, Soilmoisture Equipment Corporation, indicates a conductance of approximately 6×10^{-9} $m^2 s^{-1}$ for a new 100 kPa ceramic plate. Conductance describes the ability of the plate to transmit fluid. It is calculated by multiplying the hydraulic conductivity of the plate by the plate area and dividing by the plate thickness. Tests on the new porous plates used for outflow in this study showed plate conductance to average 4×10^{-9} $m^2 s^{-1}$. Tuff cores were expected to have a significantly lower conductance than the plates.

After vacuum-saturating the core segments, the samples were placed on the porous ceramic plate of the pressure extraction vessel, with a dampened No. 42 Whatman filter paper lying between the sample and the plate to provide a good hydraulic connection. The vessel was sealed and pressure was applied using nitrogen gas. The imposed external pressure of the gas results in an equivalent matric pressure within the core segment upon equilibration. At each pressure step, the samples were weighed to determine their volumetric moisture content, using an analytical balance accurate to one hundredth of a gram. At increasing increments, pressures of .010, .025, .050, .100, .300, and .500 MPa were applied to the cores using the method just described, and water contents were determined for the core samples.

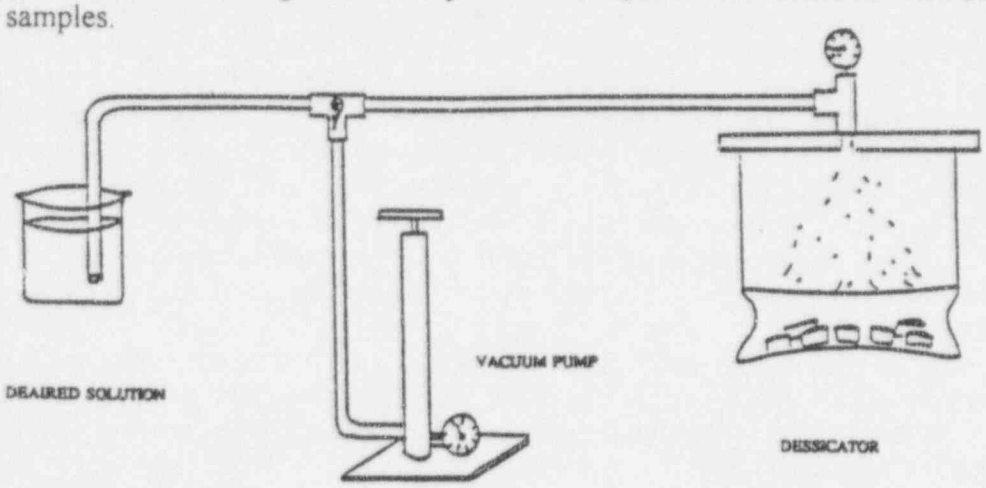

Figure 3.2 Setup for vacuum-saturating consolidated samples.

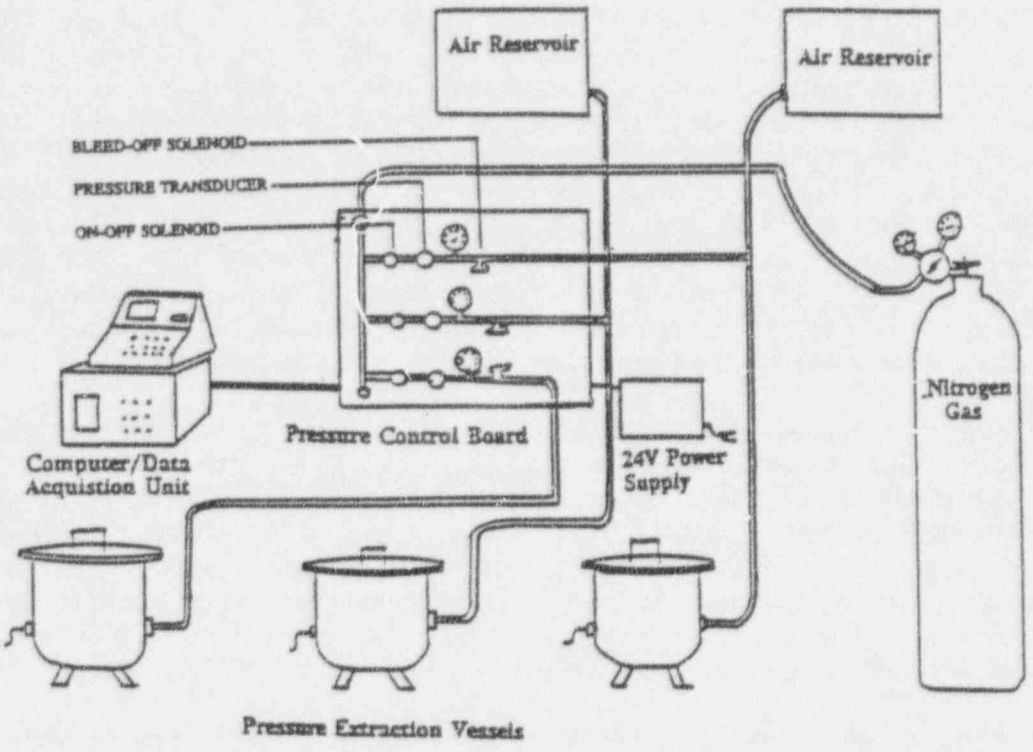

Figure 3.3. Schematic of setup for the pressurized moisture extraction vessel.

3.2 VAPOR PRESSURE EQUILIBRATION METHOD

For matric pressures greater than .500 MPa, saturated salt solutions were used to impose the desired potential on core segments, as suggested by Klute (1986). The vapor equilibration method is based on the principle that two solutions of non-volatile solutes will evaporate/condense from one to the other until their concentrations have altered sufficiently to produce equal vapor pressures between them (Robinson and Stokes, 1970). The water potential in the vapor phase associated with a saturated salt solution creates a vapor pressure gradient with respect to the potential of the moisture in the rock samples, and it is this gradient which provides the mechanism for moisture desorption and sorption. Core samples were positioned just above a saturated salt solution on a lattice, within a closed lucite dessicator chamber. This arrangement assures maximum exposed sample surface area and minimum separation between the sample and the osmotic medium, both factors in reducing equilibration time (Campbell and Gee, 1986). Equilibration time for this method was tested by running two sets of samples for each pressure step for several time periods ranging from 3 to 8 weeks. Equilibrium was determined by weighing cores at intervals of not less than seven days and was consistently attained after three weeks.

The salts used for the vapor equilibration procedure were chosen from the Handbook of Chemistry and Physics (1941), based on their matric potentials for a saturated solution at 20°C. The saturated salt solutions selected were lead nitrate, $Pb(NO_3)_2$, zinc sulfate heptahydrate, $ZnSO_4 \cdot 7H_2O$, and potassium bromide, KBr, which provide matric potentials of 2.7 MPa, 14.2 MPa, and 23.6 MPa, respectively. In each instance, saturated solutions were prepared by adding to heated water salts 20°C.

Relative humidity was measured for each solution using a hair-bundle hygrometer, with accuracy ±1%. The hygrometer was a small wall-mount type and not particularly suited to insertion into the vapor chamber, although with practice it could be done with minimum disturbance. The instrument was also subject to changes in barometric pressure. As a result, the method of hygrometer measurement was not considered to be reliable, so the theoretical potentials associated with the solutions were used to plot the moisture characteristic curves for the drier regions. Both the theoretical values and the measured values of relative humidity and water potential are listed in Table 3.1.

Table 3.1. Relative Humidity and Matric Potential for Saturated Salt Solutions: Theoretical and Measured (Hygrometer Values)

SALT	LEAD NITRATE	HYDRATED ZINC SULFATE	POTASSIUM BROMIDE
RH%			
Theoretical	98.0	90.0	84.0
Hygrometer	97.0	91.0	88.0
Potential (MPa)			
Theoretical	2.73	14.2	23.6
Hygrometer	4.12	12.8	17.3

The imbibition portion of the characteristic curve was determined by reversing the order of the matric potential equilibration steps. At the higher potentials, the cores were moved to a salt solution of less negative potential than that used for the previous step. For sorption pressure steps from .5 MPa to .01 MPa, a modified ceramic pressure plate was used, allowing core segments to imbibe de-aired solution which had been pumped through the bladder under the plate (Klute, 1986). A slow-speed peristaltic pump circulated solution from a reservoir through the plate bladder.

The methods just described for measuring desorption and sorption, which included hysteretic functions, were performed in a constant-temperature laboratory at 20° C. To investigate the effects of temperature on the moisture content vs. matric potential relationship for Apache Leap Tuff, the same 20 core segments were pressurized, in the same manner, at different temperatures. To impose the new temperature environment, the pressure extraction vessel was submerged in an insulated bath through which heated or cooled water was circulated constantly. In this manner, additional desorption data to .5 MPa were collected at 5° C and at 45° C.

3.3 PERMEAMETER/TEMPE CELL METHOD

The outflow method introduced by Gardner (1956) estimated unsaturated hydraulic conductivity by assuming that: (a) K remains constant for outflow from a small pressure increment applied to the sample, and (b) pressure plate impedence is negligible. Many refinements have since been made to Gardner's method, including plate impedence accountability (Miller and Elrick, 1958) and the variability of K after the first 10-15% of the outflow (Kunze and Kirkham, 1962). The method described by Klute (1964) is used to determine unsaturated hydraulic conductivity for this study, where K is assumed constant over the range of water contents which result from a given outflow step. The expected low conductance of the tuff core samples (Rahi, 1986; Rasmussen et al., 1990) precludes the incorporation of pressure plate impedance. The outflow method was also used to obtain data for saturated hydraulic conductivity, with slight differences in the technique as employed by Rasmussen et al. (1990). While all core segments were vacuum-saturated as before, those used for saturated hydraulic conductivity measurements were "packed" into cylinders. "Packed" cores were constructed by forcing water-proof caulking into the annular space between the rock and cylinder wall, leaving both upper and lower surfaces unobstructed (permeameter cell, Figure 3.4). This technique allows for axial flow, i.e., through the core only.

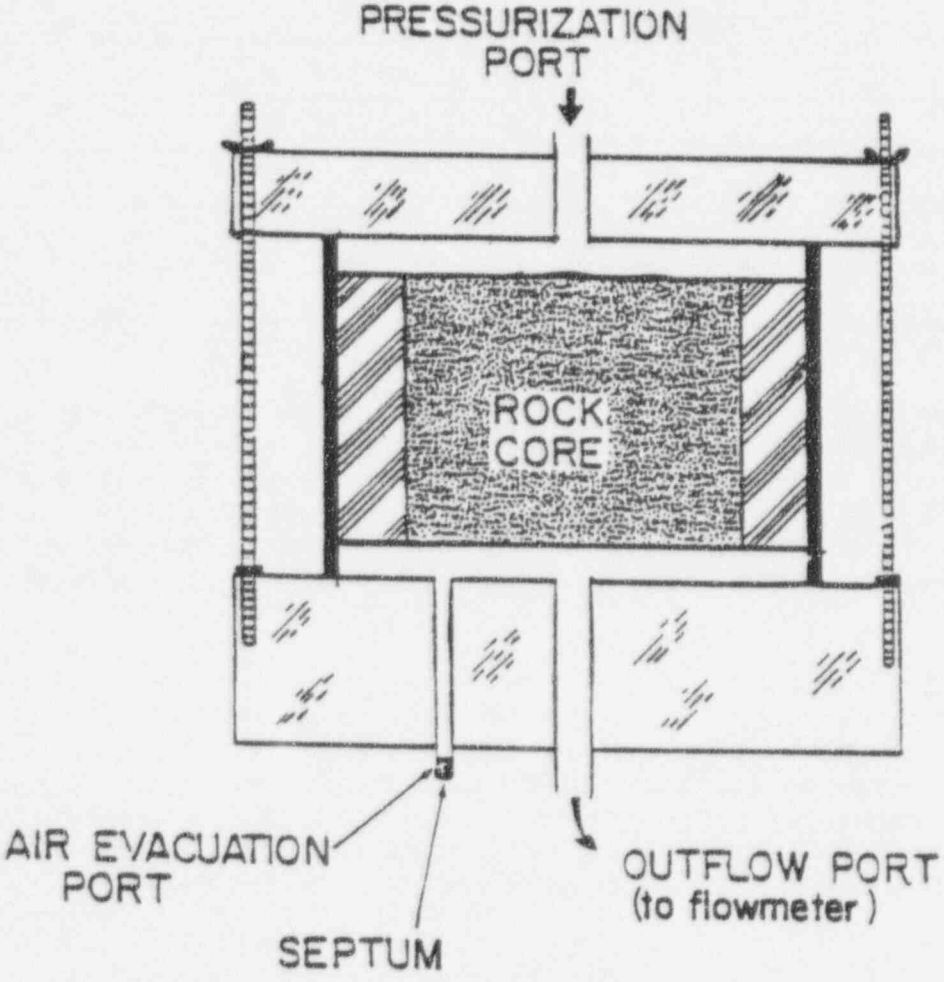

Figure 3.4. Schematic of permeameter cell.

In the constant-temperature laboratory at 20° C, a pressure increment was applied either as solution or as humidified gas to induce flow under either saturated or unsaturated conditions. For saturated hydraulic conductivity measurements, solution under a maximum pressure of .050 MPa was applied to a sample in a permeameter (Figure 3.5). When the outflow rate was steady, a small air bubble was injected into a small capacity pipette which served as a flowmeter, and the bubble movement was monitored. From the change in bubble position, the outflow rate could be calculated. Subsequently, saturated hydraulic conductivity is calculated from the relationship:

$$K_s = \frac{QL}{AH} \tag{3.2}$$

where K_s is saturated hydraulic conductivity [m/s], Q is outflow rate [m^3/s], L is sample length [m], A is sample area [m^2], and H is total head imposed on the sample [m of water]. From K, the intrinsic permeability, k_w [m^2], can also be calculated:

$$k_w = \frac{K_s \mu}{\rho g} \tag{3.3}$$

where μ is water viscosity [Pa s], ρ is density of water at the temperature of interest [kg/m^3], and g is acceleration due to gravity [m/s^2].

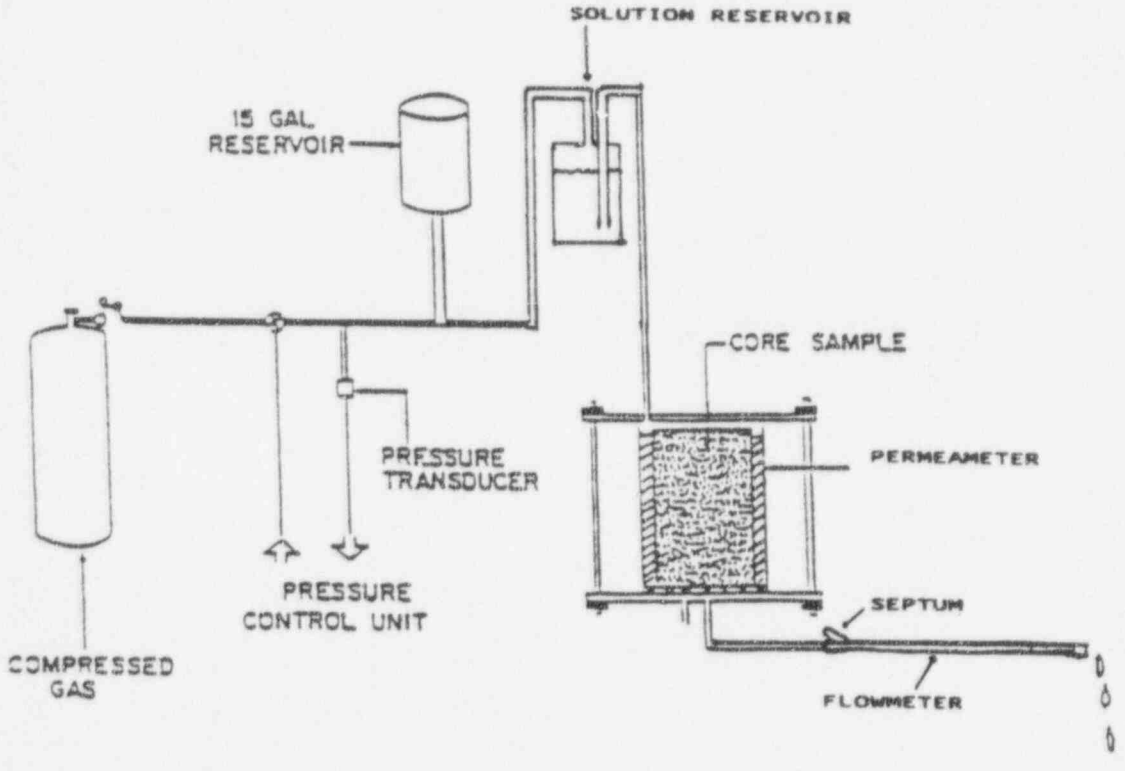

Figure 3.5. Schematic for pressurized permeameter setup.

To measure unsaturated hydraulic permeability, humidified nitrogen gas was applied to a sample in a Tempe cell, at pressures of .01, .025, .05, and .1 MPa. The rate of outflow from the pressure cell was calculated by directly measuring accumulated outflow in a calibrated buret (Figure 3.6). A peristaltic pump was used to remove gas which became trapped at the bottom of the porous plate during operation (Klute and Dirksen, 1986).

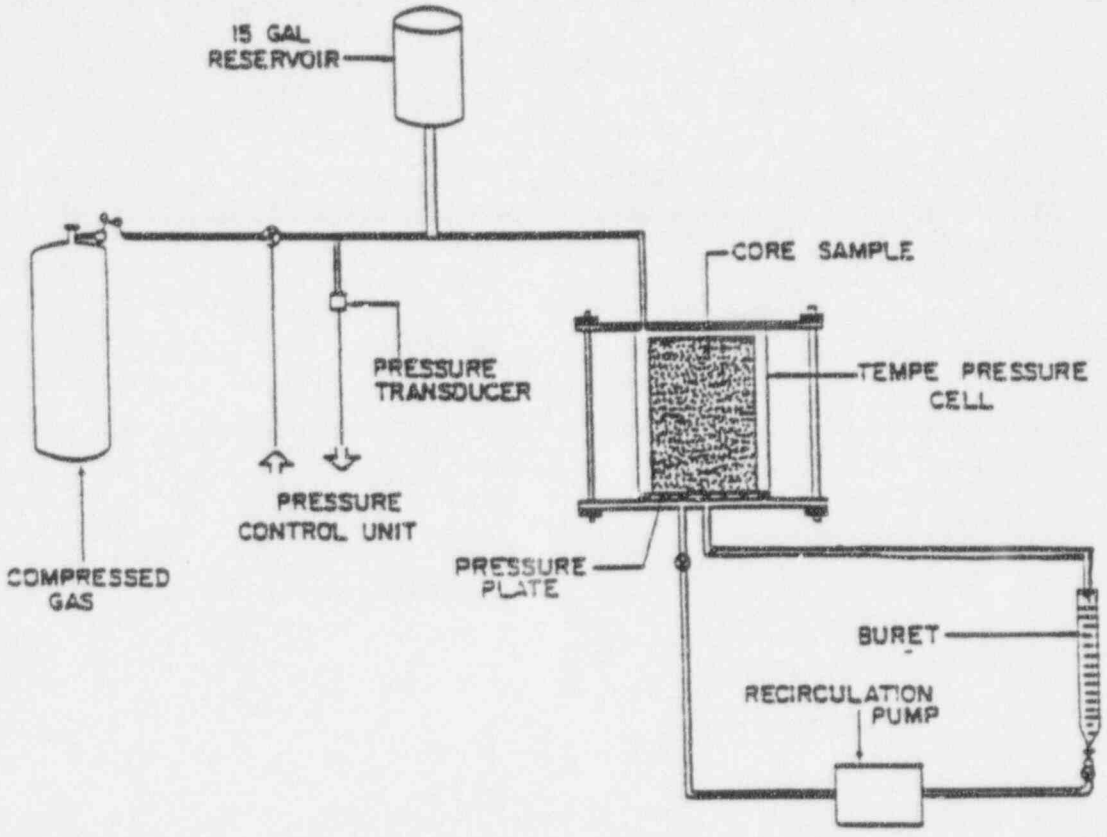

Figure 3.6. Schematic of setup for Tempe Cell method.

While the original concept of soil water diffusivity was proposed in 1950 by Childs and Collis-George, Klute (1964) provided a detailed method of solution based on theory applied to experimental measurements. An analytical form of the cumulative outflow function:

$$1 - \frac{Q(t)}{Q(\infty)} = \frac{8}{\pi^2} \sum_{m=0}^{\infty} \frac{1}{(2m+1)^2} \exp\left[\frac{-(2m+1)^2 \pi^2 Dt}{4L^2}\right] \qquad (3.4)$$

was used to calculate a table of values (Klute, 1964) for the quantities log $[Dt/4L^2]$ and log $[1 - Q(t)/Q(\infty)]$, which were then used to construct a theoretical curve, where $Q(t)$ $[m^3/s]$ is outflow at time t [s], $Q(\infty)$ is steady-state outflow rate, D is diffusivity $[m^2/s]$, and L is sample length [m]. On the same type of log-log graph paper, the quantity log $[1 - Q(t)/Q(\infty)]$ versus log t is plotted for the experimental data. A curve-matching technique is employed by translating along the log $[Dt/4L^2]$

axis only and reading the corresponding value of t from the experimental curve. If w represents the chosen value of $Dt/4L^2$ and t is the experimental value of time corresponding to the chosen value of w, then diffusivity is given by:

$$D = \frac{w4L^2}{t}. \tag{3.5}$$

For sample volume, V [m^3], the specific water capacity, C [m^{-1}], is expressed by:

$$C = \frac{Q(\infty)}{V\Delta h}, \tag{3.6}$$

and hydraulic conductivity is given by:

$$K = DC. \tag{3.7}$$

3.4 EMPLOYING THE RETC MODEL

As discussed earlier, van Genuchten's RETC program employs a curve-fitting model using the empirically derived parameters α, n, and m. Although these parameters are calculated from the measured input data, a close initial estimate significantly reduces the number of iterations required. For this study, initial estimates for α and n were taken from Rasmussen et al. (1990), who also applied the method to samples of Apache Leap Tuff. The model variable MTYPE defines the type of retention and conductivity models which are to be implemented in RETC. That is, the n and m case chosen determines the retention model to be used, and Mualem's Equation (10) or Burdine's Equation (11) model describes the conductivity model to be used. An MTYPE of 1 applies Equation (9) with variable m and n and Mualem' model. MTYPE's of 3 and 5 also employ Mualem's model, but apply Equation (9) with $m = 1 - 1/n$ and $n \rightarrow \infty$, respectively. For MTYPE 2, 4, or 6, Equation (9) with variable m and n, $m = 1-2/n$, or $n \rightarrow \infty$, respectively, are applied as the retention model and Burdine's model is used to calculate conductivity. An MTYPE of 1 was subsequently used to model data from this study. The model parameter L, which alludes to pore connectivity, has been found to average 0.5 for most soils (Mualem, 1976a). Besides the three fitting parameters and pore connectivity factor just described, the RETC program also requires initial values for residual and saturated water contents, as well as a value for saturated hydraulic conductivity. These values can be determined from the laboratory procedures detailed earlier in this section.

4. RESULTS AND DISCUSSION

Fundamental matric characteristics were measured to facilitate the eventual determination of hydraulic properties for Apache Leap Tuff. For the 20 core segments used in the derivation of the characteristic curves, the average core length was 2.51 cm, and the average volume was 71.01 cm^3 (Table 4.1). The effective porosity of the matrix material, equivalent to the saturated water content at zero pressure, is defined as the volume of interconnected voids per unit volume of rock. To determine this parameter, the difference in mass between each vacuum-saturated and oven-dried sample was divided by the density of water and the volume of the sample. Supplementary data, including procedures, for thermal conductivity are contained in Appendix B.

Table 4.1. Basic Information for Samples at 20° C.

Sample #	Dry Weight (g)	Saturated Weight (g)	Volume (ccm)	Height (cm)	Porosity
0701	153.80	167.56	71.53	2.53	0.1647
0702	152.28	164.29	69.27	2.45	0.1737
0703	155.17	165.41	69.27	2.45	0.1481
0704	154.12	165.35	70.12	2.48	0.1604
0705	154.46	165.73	69.55	2.46	0.1623
0706	151.60	163.60	69.27	2.45	0.1779
0707	155.05	165.93	69.27	2.45	0.1573
0708	160.44	171.49	71.82	2.54	0.1541
0709	153.16	164.78	69.27	2.45	0.1681
0710	148.49	159.85	67.56	2.39	0.1670
0711	161.05	172.75	71.82	2.54	0.1632
0712	160.62	172.77	73.23	2.59	0.1662
0713	161.55	174.48	74.36	2.63	0.1742
0714	156.61	168.30	70.69	2.50	0.1657
0715	160.59	172.63	70.69	2.50	0.1706
0716	159.51	172.31	72.10	2.55	0.1779
0717	157.60	169.36	70.97	2.51	0.1660
0718	162.77	174.68	72.67	2.57	0.1642
0719	168.24	180.45	75.78	2.68	0.1614
0720	157.72	170.25	70.97	2.51	0.1769

4.1 MOISTURE RETENTION EXPERIMENT RESULTS

As many as 20 saturated core segments were allowed to equilibrate under pressure at 20° C, resulting in the statistical summaries of water content and relative saturation listed in Tables 4.2 and 4.3, respectively. The pressure plate extractor was used for pressures less than or equal to .5 MPa and required up to seven days to attain equilibrium for a single pressure step at 20° C. For pressures greater than .5 MPa, core segments were enclosed with an appropriate saturated salt solution until equilibrium was reached. Although this method was tested by running two sets of samples for several time periods ranging from 3 to 8 weeks for each solution/equilibration pressure, equilibrium was consistently attained after 3 weeks. The reader is reminded that equilibration time is a function of sample size and, therefore, the smallest representable size is recommended. The vapor equilibration method is reliable, but may pose a serious limitation due to the long time periods required at high pressures.

The same pressures were applied in reverse order to effect matrix moisture absorption. Both pressurized vessel and salt solution methods were used to generate data for the main drying and wetting portions of the moisture characteristic curve at 20° C. The pressurized moisture extraction vessel alone was used to generate data for three hysteresis scanning curves and retention data at both 45° C and 5° C.

Mean values of relative saturation were plotted against matric potential to produce retention curves and three hysteresis scanning curves. Note that all data points for observed data plots were based on the arithmetic means of ten or 20 samples, with the exception of K_{sat}, which was based on a median value of ten samples. The analysis reveals a coefficient of variation of less than 2.2% for retention data at all matric potentials, desorbing or sorbing, at 20° C. Similarly, the coefficients of variation for 45° C and 5° C were less than 4.2% and 1.2%, respectively. The small value of the coefficient of variation indicates both small geologic variation within the sample set and small measurement error within the experimental group.

In the observed data plot shown in Figure 4.1, the main imbibition curve somewhat parallels the main drying curve, except at the lowest water contents, where one can see a greater change in pressure head with change in water content for the sorption curve than that evidenced by the desorption curve. This phenomenon is consistent with other imbibition experiments (Lenhard et al., 1991; Poulovassilis, 1970). As with the moisture retention curves developed for other rock samples (Flint, 1993), the characteristic curves in Figure 4.1 exhibit a broader, more blunt shape than the sigmoidal shapes typical of granular porous media (Stonestrom and Rubin, 1989). Figure 4.2 shows a characteristic curve representative of porous granular media for comparison. The generally broader shape associated with the tuff is most likely a result of air entrapment during the wetting process. On the other hand, the wide separation between branches of the retention curve at the very dry end may be due to the peculiarities associated with vapor transport, such as adsorption and diffusion.

The first hysteresis scanning curve was derived by desorbing saturated cores to equilibrium at .5 MPa, then allowing them to imbibe moisture to equilibrium at .010 MPa. The set of data for this hysteresis curve was obtained from a third set of ten core segments, for which initial saturated water content (Table 4.4) was somewhat lower than that for the first 20 samples. The difference was probably due to the subsequent "flushing" of the first set of samples, which increased the effective porosity. This phenomenon of possible clay particle removal will be explained later. Because of that initial difference, these curves were normalized by plotting the mean values of relative saturation (Table 4.5). The first scanning curve is plotted in Figure 4.1 with the main drying and imbibition curves. The divergence from the main drying branch makes obvious the effects of air entrapment. Stonestrom and Rubin (1989) found similar results with sand and loam

Table 4.2. Statistical Summary of Water Contents (ccm/ccm) for ALT desorbing/absorbing at 20°C.

	Matric Potential (MPa)									
	0.0	0.01	0.025	0.050	0.10	0.30	0.50	2.73	14.24	23.57
Desorption:										
# Repetitions	20.0	20.0	20.0	20.0	20.0	20.0	20.0	20.0	20.0	20.0
Mean	0.1660	0.1611	0.1596	0.1552	0.1396	0.1112	0.0858	0.0579	0.0302	0.0226
Coefficient Variation	0.0106	0.0109	0.0103	0.0092	0.0109	0.0186	0.0166	0.0103	0.0135	0.0108
Minimum	0.1481	0.1430	0.1423	0.1426	0.1208	0.0905	0.0759	0.0540	0.0270	0.0207
Median	0.1658	0.1618	0.1600	0.0155	0.1416	0.1114	0.0844	0.0577	0.0300	0.0225
Maximum	0.1779	0.1740	0.1722	0.1660	0.1507	0.1283	0.0970	0.0626	0.0345	0.0251
Absorption:										
# Repetitions	--	10.0	10.0	10.0	10.0	10.0	20.0	20.0	20.0	--
Mean	--	0.1355	0.1291	0.1151	0.0944	0.0751	0.0604	0.0278	0.0245	--
Coefficient Variation	--	0.0141	0.0123	0.0140	0.0183	0.0218	0.0209	0.0113	0.0104	--
Minimum	--	0.1282	0.1227	0.1060	0.0858	0.0683	0.0506	0.0249	0.0221	--
Median	--	0.1337	0.1277	0.1149	0.0942	0.0738	0.0608	0.0278	0.0244	--
Maximum	--	0.1455	0.1371	0.1228	0.1005	0.0855	0.0720	0.0310	0.0269	--

Table 4.3. Statistical Summary of Relative Saturations (%) for ALT desorbing/absorbing at 20°C.

	Matric Potential (MPa)								
	0.10	0.025	0.050	0.10	0.30	0.50	2.73	14.24	23.57
Desorption:									
# Repetitions	20.0	20.0	20.0	20.0	20.0	20.0	20.0	20.0	20.0
Mean	97.08	96.17	93.55	84.18	67.04	51.82	34.96	18.25	13.63
Coefficient Variation	0.0029	0.0025	0.0043	0.0099	0.0178	0.0210	0.0187	0.0188	0.0181
Minimum	94.21	93.59	89.43	78.36	58.46	45.31	31.23	15.80	12.20
Median	97.32	96.43	93.87	83.68	66.99	51.23	33.61	17.79	13.37
Maximum	98.54	97.81	96.29	90.55	76.78	60.58	41.39	21.14	16.00
Absorption:									
# Repetitions	10.0	10.0	10.0	10.0	10.0	20.0	20.0	20.0	--
Mean	83.14	79.21	70.58	57.86	46.01	37.08	17.08	14.80	--
Coefficient Variation	0.0203	0.0183	0.0188	0.0206	0.0200	0.0222	0.0187	0.0167	--
Minimum	77.43	73.63	63.96	50.55	39.32	30.72	14.90	13.32	--
Median	81.64	77.73	69.96	57.77	46.35	37.92	17.06	14.51	--
Maximum	95.81	89.33	77.85	63.47	49.66	44.36	19.04	16.94	--

Table 4.4. Statistical Summary for Hysteresis Sorbing from 0.5 MPa-Water Content (ccm/ccm)

	Matric Potential (MPa)					
	0.10	0.025	0.050	0.100	0.300	0.500
# Repetitions	10.0	10.0	10.0	10.0	10.0	10.0
Mean	0.1317	0.1254	0.112	0.1017	0.0917	0.0838
Coefficient Variation	0.0106	0.0191	0.0190	0.0219	0.0278	0.0248
Minimum	0.1250	0.1074	0.1021	0.0919	0.0829	0.0753
Median	0.1319	0.1287	0.1113	0.1003	0.0887	0.0842
Maximum	0.1366	0.1334	0.1241	0.1132	0.1048	0.0958

Table 4.5. Statistical Summary for Hysteresis Sorbing from 0.5 MPa-Relative Saturation (%).

	Matric Potential (MPa)					
	0.01	0.025	0.050	0.100	0.300	0.500
# Repetitions	10.0	10.0	10.0	10.0	10.0	10.0
Mean	92.77	88.30	78.88	71.70	64.74	59.08
Coefficient Variation	0.805	1.43	1.8	2.35	3.38	2.54
Minimum	87.78	79.85	72.25	62.83	54.32	51.46
Median	92.85	89.47	78.57	71.99	64.35	61.15
Maximum	96.46	92.32	84.25	78.09	78.92	65.93

samples, where significant air entrapment occurred only after saturation levels greater than 70% of the effective porosity were achieved upon imbibition.

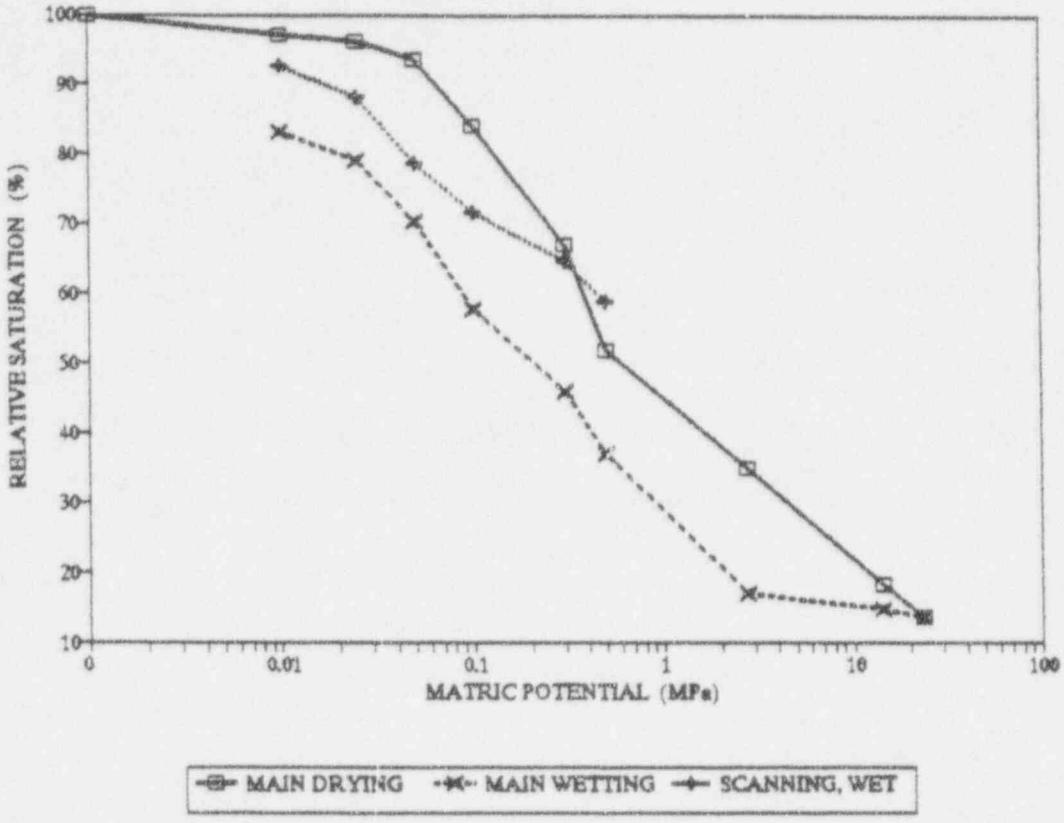

Figure 4.1. Moisture retention curves for ALT with a single hysteresis scanning curve at 20° C.

A second set of hysteresis scanning curves (Figure 4.3) were produced by reversing the order of applied pressure steps immediately upon sorption equilibration of the main wetting curve at .01 MPa. The scanning curves are seen to reflect the imbibition curve and indicate the same closed-loop behavior found by Lenhard et al. (1991). Such behavior implies that very little additional air entrapment occurred during this cycle of wetting/drying/wetting. A summary of water content and relative saturation data for the last set of scanning curves can be found in Tables 4.6 and 4.7. Complete data sets for moisture retention at 20° C, including all hysteresis scanning curves, can be found in Appendix A, Tables A1 through A6.

Comprehensive moisture characterization data were collected at 20° C before the moisture extraction vessel method was applied at first 45° C and then 5° C. During the process of oven-drying and resaturation for these repeated experiments, it is possible that small clay particles or bacteria were dislodged within the rock matrix, although there was no physical evidence of this explanation. This "flushing" phenomenon was most likely the cause of the apparent increase in effective porosity, from an initial porosity of 0.1463, as exemplified by the hysteresis data in Table 4.4, to 0.1660 for the data obtained at 20° C, and to approximately 0.1740 for the data obtained at both 45° and 5° C. Statistical summaries for water content data at these last two temperatures can be found in Tables 4.8, 4.10; statistical summaries for relative saturation are listed in Tables 4.9

and 4.11. Complete sets for data at 45° C can be found in Tables A7 and A8; complete sets for data at 5° C are presented in Tables A9 and A10.

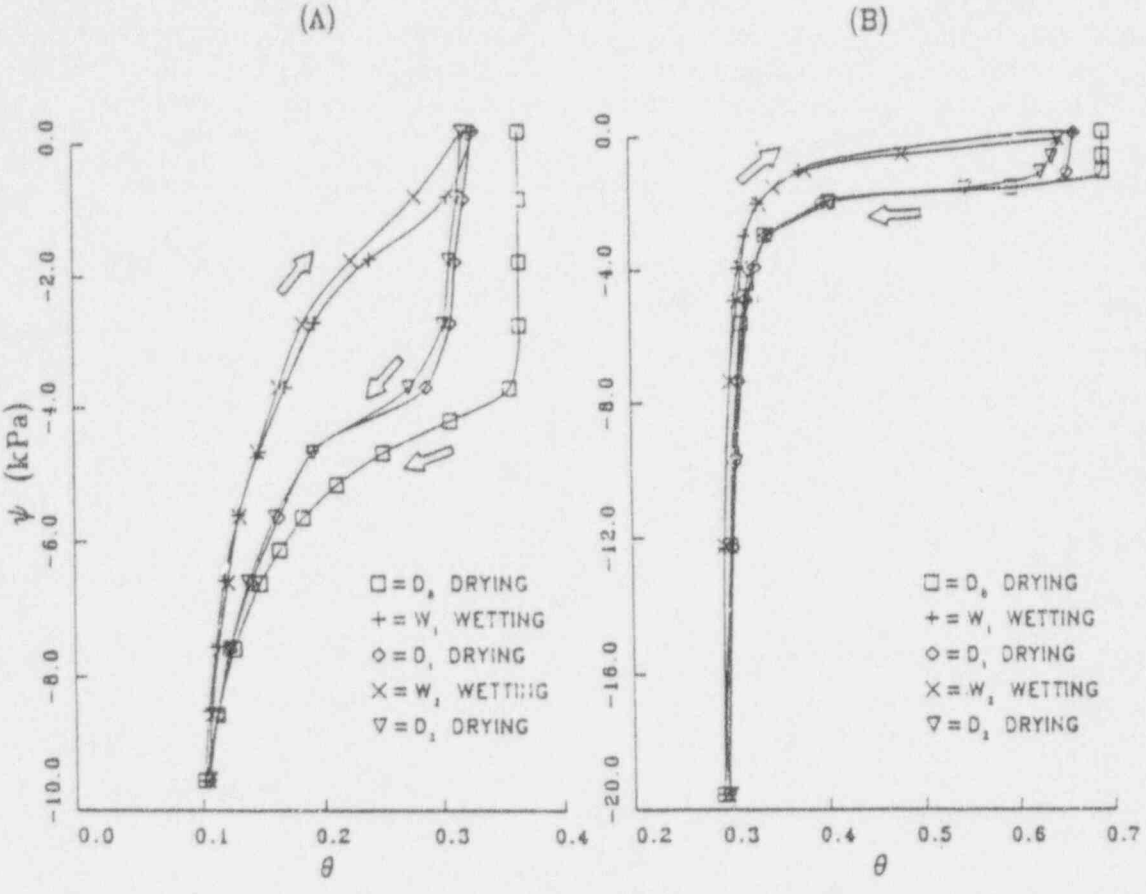

Figure 4.2. Representative characteristic curves for unconsolidated porous media: (A) Oakley sand, (B) Aiken aggregates (from Stonestrom and Rubin, 1989).

To determine where the increased moisture may be stored within the matrix material, a pore-size distribution analysis was done based on data from the three temperature sets. Figure 4.4 is a graph of the moisture retention curve at 20° C with the pore size classes sketched in. The point of division for pore classes was determined by the change in slope of the desorption curve, the assumption being that a class of smaller pores will require a detectable decrease in matric potential. For this somewhat subjective determination, the average pore radius was calculated for each size range based on the mean water content for each range. Note that step sizes in water content only reflect the number of pores within each size range. The step size associated with the class one pores is approximately 0.0240 for data at 20° and 0.032 for the other temperature data sets. The step size associated with class two pores is approximately 0.06 for the data at 20° and 0.08 for the data at the other temperatures, for which the "flushed" cores had an increased water content. The apparent increased step size, smaller for class one pores than for class two pores, indicates that most of the extra moisture was probably held in the pores of class two size range. Using the well-known relationship:

$$r = \frac{-2\sigma}{\rho_l g h_m} \tag{4.1}$$

where r is pore radius [m], σ is surface tension [N/m], g is gravity [N/kg], ρ_w is density of water [kg/m^3], and h_m is potential in meters, the average pore size radius for each class can be calculated. The average pore radius for the class one group falls in the range of 2.1 to 3.1 μm; for the class two group, .55 to .795 μm; and for the class three group of the 20° data, approximately .1 μm.

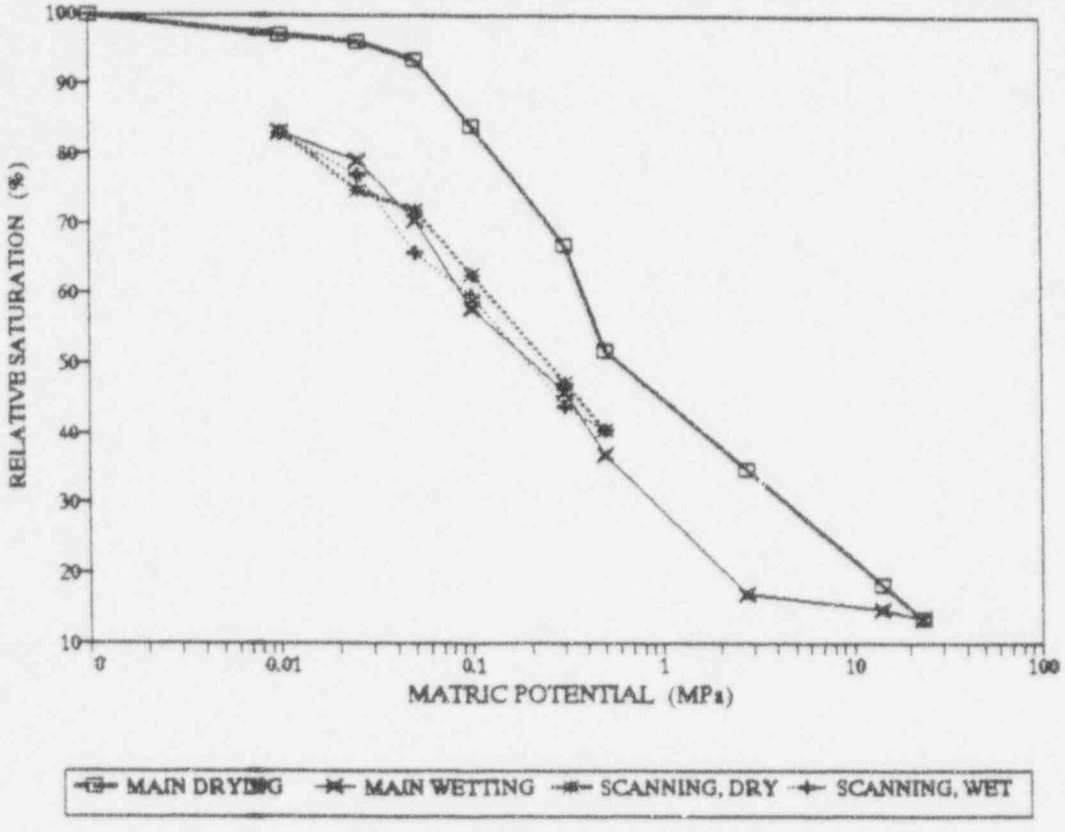

Figure 4.3. Moisture retention curves for ALT with hysteresis scanning loop at 20°.

4.2 MODELING RESULTS

Desorption data from experiments at 5°, 20°, and 45° C were fitted using the curve-fitting model RETC, as revised by van Genuchten et al. (1991). In each case, the variable MTYPE was set at one, which applies Mualem's model, as defined by Equation (10), with variable m and n. For this study, only retention data were entered as input. Of the seven parameters for which initial input was required, the model held the input value as constant for residual water content [WCR], pore-connectivity [L] (i.e., Mualem's parameter *l*), and saturated hydraulic conductivity [K]. WCR was set to zero, and saturated K was set to 0.0004, 0.0006, and 0.0002 meters per day for data at 20°, 45°, and 5° C, respectively. While Mualem (1976a) found *1* [L] to be approximately 0.5 for most soils, the tortuousity factor for the matrix material studied here is expected to be greater than that for soils, and the pore-connectivity value lower. When the RETC model was applied to

Table 4.6. Statistical Summary for Hysteresis Loop at 20° C, Desorbing to/ Absorbing from 0.5 MPa, Water Content (ccm/ccm).

	Matric Potential (MPa)					
	0.10	0.025	0.050	0.100	0.300	0.500
Desorption:						
# Repetitions	--	10.0	10.0	10.0	10.0	10.0
Mean	--	0.1261	0.1215	0.1056	0.0798	0.0685
Coefficient Variation	--	0.0128	0.0135	0.0180	0.0159	0.0134
Minimum	--	0.1190	0.1132	0.0944	0.0733	0.0639
Median	--	0.1257	0.1217	0.1055	0.0802	0.0688
Maximum	--	0.1335	0.1297	0.1146	0.0865	0.0726
Absorption:						
# Repetitions	10	10	10	10	10	10
Mean	0.1391	0.1298	0.1112	0.1007	0.0739	--
Coefficient Variation	0.0126	0.0133	0.0162	0.0111	0.0126	--
Minimum	0.1320	0.1207	0.1029	0.0954	0.0694	--
Median	0.1377	0.1301	0.1117	0.1012	0.0743	--
Maximum	0.1490	0.1382	0.1201	0.1055	0.0780	--

Table 4.7. Statistical Summary for Hysteresis Loop at 20° C, Desorbing to/ Absorbing from 0.5 MPa, Relative Saturation (%)

	Matric Potential (MPa)					
	0.10	0.025	0.050	0.100	0.300	0.500
Desorption:						
# Repetitions	--	10.0	10.0	10.0	10.0	10.0
Mean	--	74.79	72.06	62.67	47.33	40.66
Coefficient Variation	--	0.0067	0.0102	0.0171	0.0157	0.0154
Minimum	--	71.69	68.32	56.97	44.24	38.49
Median	--	75.09	72.30	62.61	46.98	40.80
Maximum	--	77.27	76.41	69.30	50.86	44.30
Absorption:						
# Repetitions	10	10	10	10	10	--
Mean	82.95	76.99	65.97	59.74	43.88	--
Coefficient Variation	0.0063	0.0096	0.0142	0.0092	0.0149	--
Minimum	79.52	72.71	62.10	57.57	41.45	--
Median	83.48	77.44	64.23	59.18	43.95	--
Maximum	84.70	80.02	69.67	62.56	47.79	--

Table 4.8. Statistical Summary for Water Contents (ccm/ccm) at 45° C.

	Matric Potential (MPa)					
	0.10	0.025	0.050	0.100	0.300	0.500
Desorbing:						
# Repetitions	20.0	20.0	20.0	20.0	20.0	20.0
Mean	0.1698	0.1671	0.1592	0.1211	0.0703	0.0683
Coefficient Variation	0.0356	0.0392	0.0304	0.0181	0.0116	0.0091
Minimum	0.1485	0.1447	0.1429	0.1073	0.0619	0.0622
Median	0.1616	0.1594	0.1493	0.1210	0.0710	0.0684
Maximum	0.1687	0.1680	0.1589	0.1456	0.0748	0.0727

Table 4.9. Statistical Summary of Relative Saturations at 45° C.

	Matric Potential (MPa)					
	0.10	0.025	0.050	0.100	0.300	0.500
Desorbing:						
# Repetitions	20.0	20.0	20.0	20.0	20.0	20.0
Mean	92.51	91.07	85.70	69.47	40.32	39.16
Coefficient Variation	0.0082	0.0086	0.0070	0.0116	0.0116	0.0091
Minimum	85.19	83.01	81.96	61.56	35.51	35.68
Median	93.21	91.67	85.33	69.43	40.82	39.40
Maximum	96.78	96.36	91.17	83.52	42.94	41.72

Bandelier Tuff, L ranged from .49 to -1.1 (van Genuchten et al., 1991). After experimenting with the model, the parameter L was set to 0.3, and a better fit was accomplished. The other parameters were allowed to vary as needed by the curve-fitting process. Table 4.12 lists the RETC parameters ultimately used to fit the data for the three temperatures.

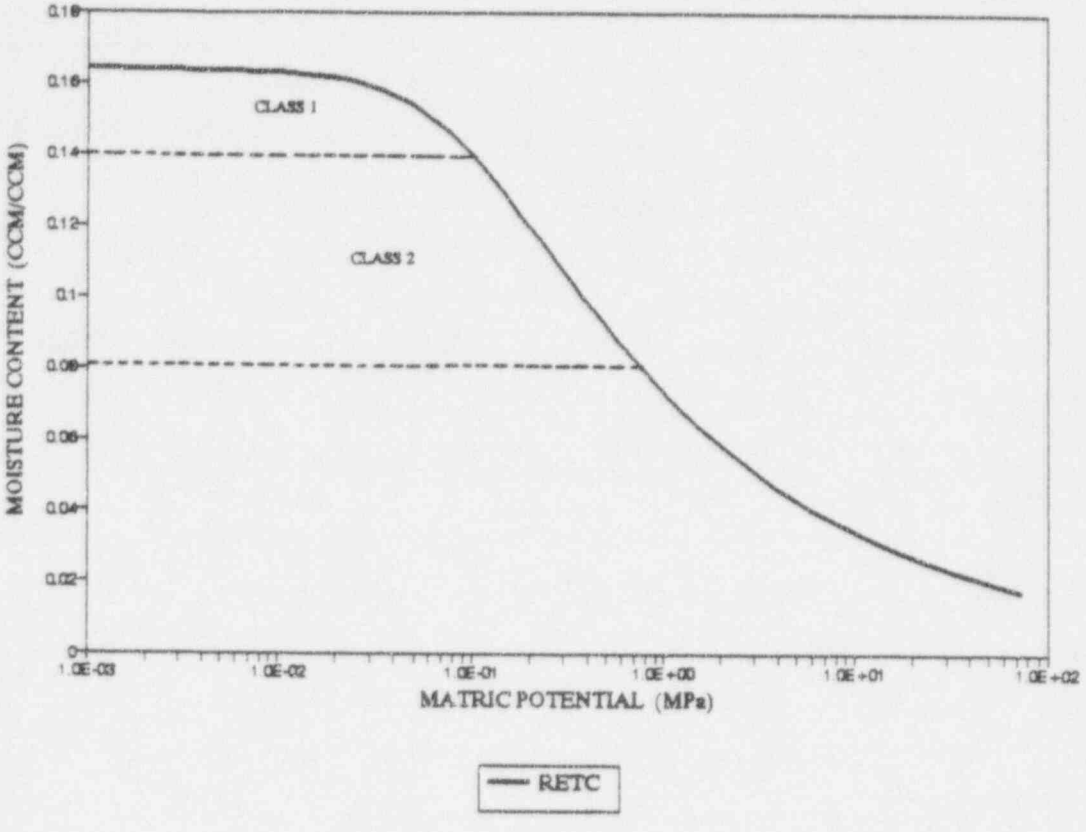

Figure 4.4. ALT characteristic curve at 20° with pore class designations sketched in.

4.2.1 Moisture Retention Curves

Results of the RETC model for data at each experimental temperature of 20°, 45°, and 5° are plotted with the mean empirical values for water content at their corresponding matric potentials. Data for all three temperatures were collected at matric pressure equivalents of 0.01, 0.025, 0.05, 0.1, 0.3, and 0.5 MPa, while additional data were collected at 20° C for equivalent pressures of 2.73, 14.2, and 23.6 MPa. The fitted desorption curve at 20° C is shown with the associated observation points in Figure 4.5. The goodness-of-fit is designated by an R-squared of 0.9965. Fitted values and observations at 45° and 5° C are plotted in Figures 4.6 and 4.7. Again, goodness-of-fit is designated by R-squares of 0.9921 and 0.9954 for results at 45° and 5° C, respectively.

Changes in pressure head due to temperature changes are generally predicted based on a solution proposed by Philip and de Vries (1957), employing a temperature coefficient of pore water pressure head contingent upon temperature-dependent changes in the surface tension of pure water. Several researchers, including Haridasan and Jensen (1972), Wilkinson and Klute (1962),

Table 4.10. Statistical Summary of Water Contents (ccm/ccm) at 5° C.

	Matric Potential (MPa)					
	0.10	0.025	0.050	0.100	0.300	0.500
Desorbing:						
# Repetitions	20.0	20.0	20.0	20.0	20.0	20.0
Mean	0.1732	0.1690	0.1613	0.1226	0.0854	0.0769
Coefficient Variation	0.0095	0.0092	0.0080	0.0115	0.0078	0.0074
Minimum	0.1541	0.1509	0.1436	0.1104	0.0778	0.0712
Median	0.1738	0.1711	0.1621	0.1213	0.0861	0.0777
Maximum	0.1836	0.1783	0.1725	0.1377	0.0888	0.0805

Table 4.11. Statistical Summary of Relative Saturations (%) at 5° C.

	Matric Potential (MPa)					
	0.10	0.025	0.050	0.100	0.300	0.500
Desorbing:						
# Repetitions	20.0	20.0	20.0	20.0	20.0	20.0
Mean	99.09	96.68	92.31	70.16	48.93	44.05
Coefficient Variation	0.0025	0.0055	0.0056	0.0098	0.0118	0.0122
Minimum	95.76	88.71	88.36	63.37	44.48	39.91
Median	99.56	97.52	92.81	70.14	49.17	44.25
Maximum	99.99	98.75	96.02	75.76	54.30	49.60

Table 4.12. RETC Model Parameters.

Case	20°	45°	5°
WCR	.0000	.0000	.0000
WCS	.1640	.1708	.1724
ALPHA	1.094	2.322	2.535
N	1.651	5.412	15.83
M	.2024	.0759	.0212
L	.3000	.3000	.3000
K	.0004	.0006	.0002
R^2	.9965	.9921	.9954

Table 4.13. Statistical Summary for Intrinsic Permeability at 20° C (m sq).

	Matric Potential (MPa)				
	0 (sat)	.010	.025	.050	.100
# Repetitions	10	5	2	3	13
Mean	1.81E-15	4.15E-15	6.95E-17	1.78E-17	6.29E-18
Coefficient Variation	7.45E-01	8.64E-02	6.48E-03	8.30E-01	2.90E-01
Minimum	3.05E-16	7.33E-16	6.90E-17	2.76E-18	9.19E-19
Median	4.30E-16	1.21E-15	6.95E-17	3.22E-18	3.20E-18
Maximum	1.39E-14	1.53E-15	6.99E-17	4.73E-17	2.44E-17

and Hopmans and Dane (1986) found the solution inadequate to predict the changes in pore pressure head which occurred with increases in temperature. Hopmans and Dane suggested that neither changes in the volume of entrapped air nor the effects of chemicals in the pore solution on surface tension could completely explain the significant effects of temperature on moisture retention curves. Nevertheless, predictions of the change in matric potential for a given water content with change in temperature invariably give an increase in potential with increase of temperature.

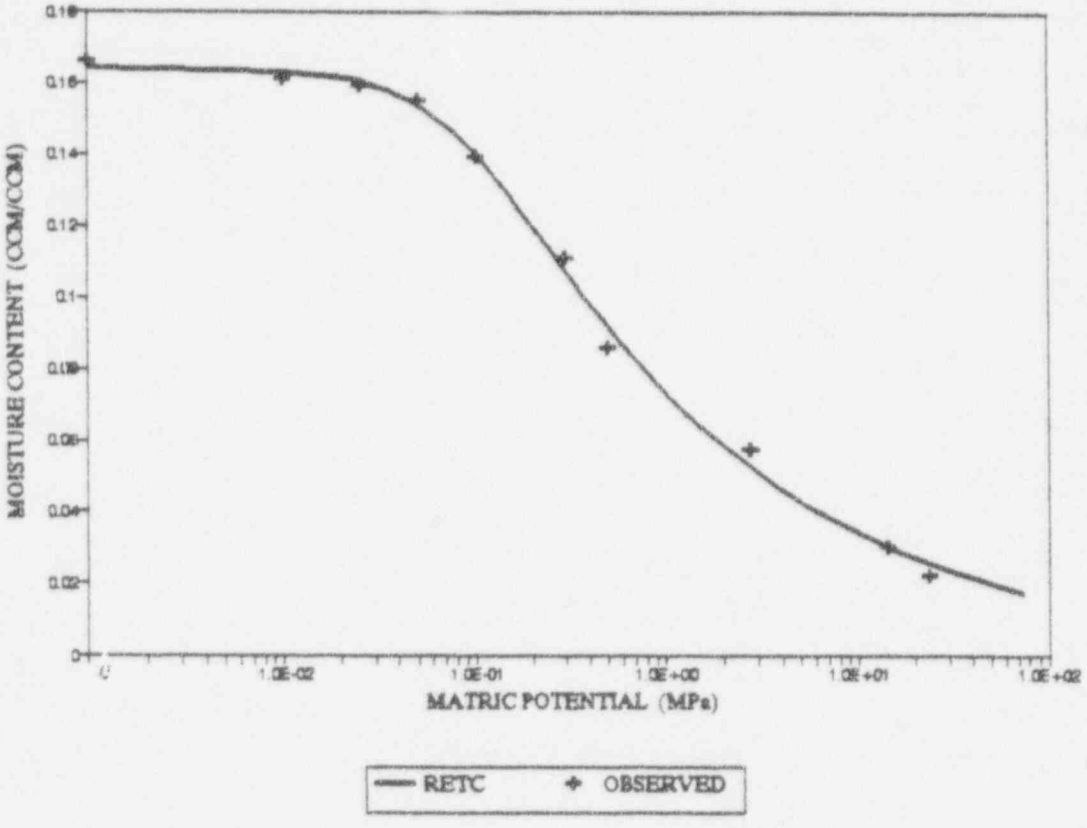

Figure 4.5. Moisture retention curve at 20°. RETC-calculated versus mean laboratory-measured values.

For this experiment, values from all three temperatures were plotted as a function of relative saturation for comparison in Figure 4.8. As expected, a temperature increase from 20° to 45° Centigrade caused the moisture retention curve to shift distinctly to the left, so that the potential at a given water content also increased. The close clustering of points representing different temperatures at the highest matric potentials is not unreasonable. Working with soils, Wilkinson and Klute (1962) and Haridasan and Jensen (1985) found relatively small differences with temperature in water contents near saturation. For the Apache Leap Tuff samples, temperature effects began to become apparent at approximately 93% relative saturation. It is readily observed that values for retention at 5° C represent water contents at matric potentials considerably higher than were expected. The points representing 5° C retention values should lie to the right of those points representing 20° C retention values. One cause for the discrepancy is experimental error, which may have been caused by an inability to detect the true point of water content equilibrium

for a given pressure step. The small, continual losses accrued during efforts to attain equilibrium may have resulted in water contents considerably lower than expected.

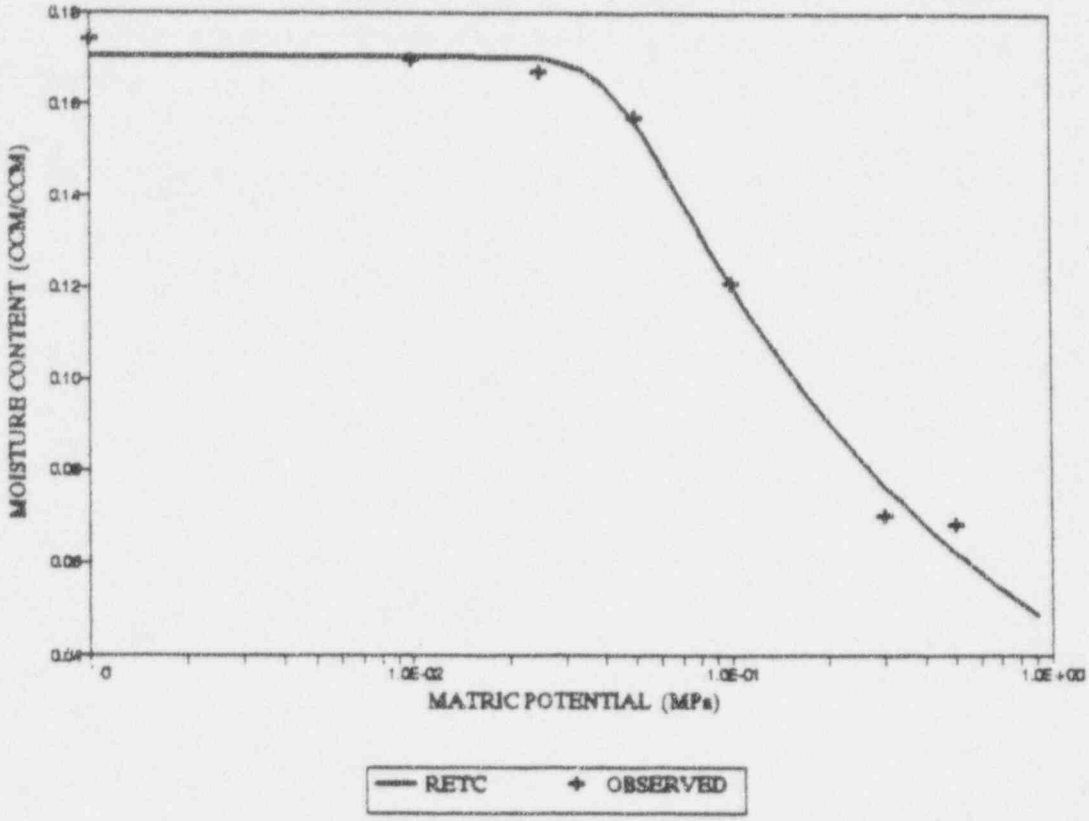

Figure 4.6. Moisture retention curve at 45° C. RETC-calculated and mean laboratory-measured values.

4.2.2 Hydraulic Conductivity Curves

The experimental values of hydraulic conductivity, used both for RETC model input as saturated hydraulic conductivity and for comparison with calculate K's, were obtained from outflow measurements taken at 20° C. Table 4.13 shows a statistical summary of hydraulic conductivity in the form of intrinsic permeability, k [m^2]. An examination of Table A.11 (the complete list of saturated permeability data) reveals that, out of ten samples, nine had values on the order of 10^{-16}. In this case, the median is a more representative value of the central tendency than the arithmetic mean. The general trend of the measured hydraulic permeability is to decrease less than an order of magnitude with each pressure step increase, with the exception of the first step at .01 MPa. At that pressure, only one sample appeared to exhibit the expected permeability rate (Table A.12), while other samples were measured at rates of one to two orders of magnitude higher. Air trapped in the Tempe cell may result in apparently greater magnitude of outflow. Trapped air may also block outflow, causing considerable underestimation of the magnitude of the outflow rate. It is expected that measurement error had significant impact on the observed unsaturated hydraulic permeability data.

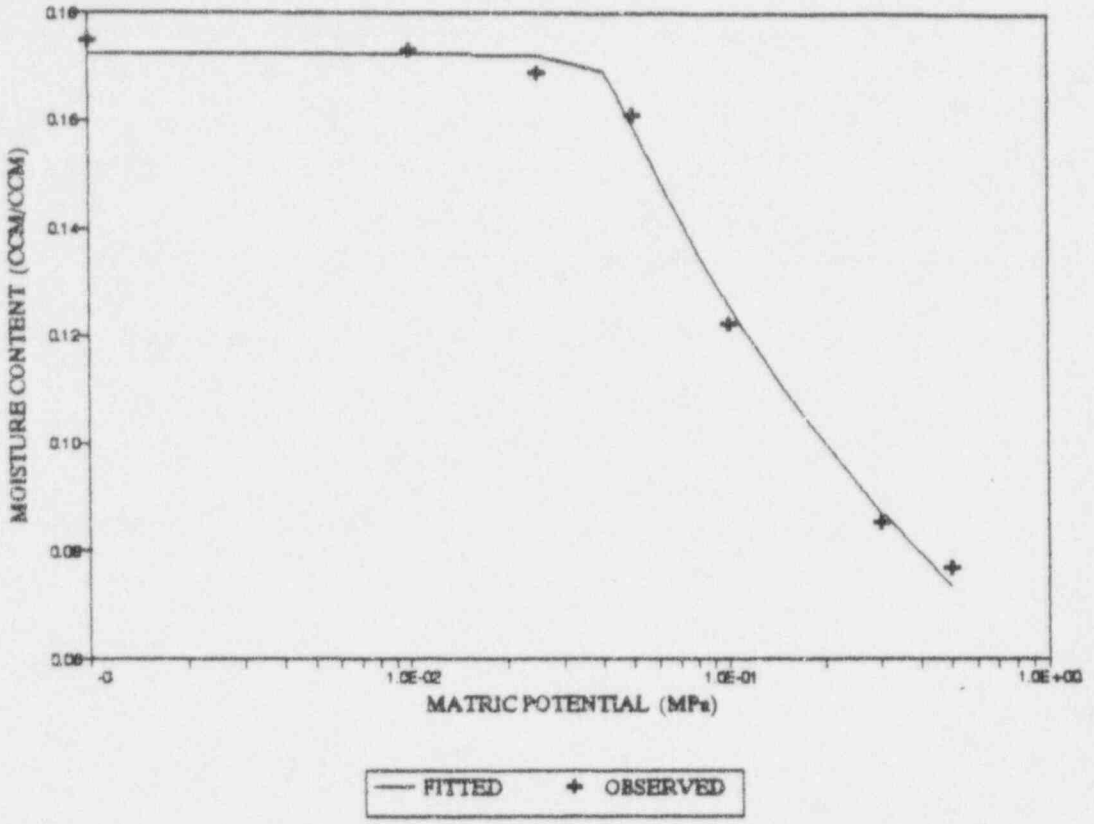

Figure 4.7. Moisture retention curve at 5°. RETC-calculated and mean laboratory-measured values.

The RETC model incorporates the measured saturated hydraulic conductivity to ultimately calculate a value of $K(\theta)$ for each value of moisture content and potential calculated during the generation of the moisture retention curve. The calculated values of K, in meters per second, are plotted with the observed values against moisture content in Figure 4.9. for data at 20° C. With the exception of the anomalous point associated with the .010 MPa pressure step, the remaining observed values, although consistently lower, follow the trend of the fitted hydraulic conductivity curve. For the purpose of evaluating the observed and/or the calculated hydraulic conductivities, both sets of values were also plotted with Apache Leap Tuff K data observed by Rasmussen et al. (1990) in Figure 4.10. The remarkable agreement between the observed data from Rasmussen et al. and the model-calculated K's indicates that the observed data from this experiment contained measurement error and that the model-calculated curve provided a reasonable description of unsaturated hydraulic conductivity for Apache Leap Tuff at 20° C. Note that, although the model calculates K for the entire range of moisture contents, values are plotted above 0.08, the approximate moisture content associated with the 0.5 MPa potential which was the limit for liquid flow for this experiment.

The viscosity ratio was the predictive method chosen for this investigation, and Equation (14) was applied to calculated K_{20} values. The resulting estimations are plotted with the calculated hydraulic conductivities at 20° and 45° C in Figure 4.11. It is obvious that the predictive curve underestimates K_{45} by as much as one order of magnitude for pertinent relative saturations of 50 to 100%. While Hopmans and Dane (1986) and Haridasan and Jensen (1972) found good correlation between observed hydraulic conductivities and predictions based on viscosity ratios, Constantz (1982) and other researchers (Nimmo, 1983) also found a temperature dependence for

K(θ) at least one order of magnitude larger than that predicted by the temperature dependence of the viscosity of water. The viscosity ratio was not applied to the K values calculated from the obviously erroneous 5° retention data.

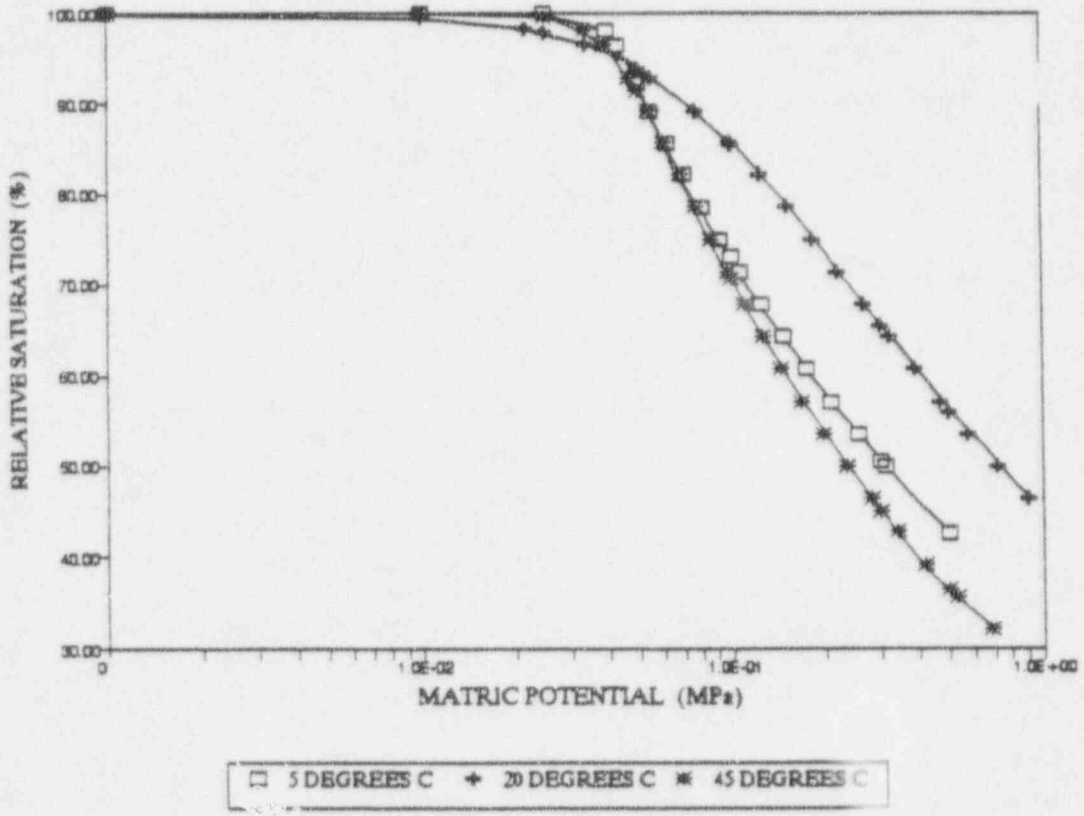

Figure 4.8. Comparison of retention curves at 5, 20, and 45° C: relative saturation versus matric potential.

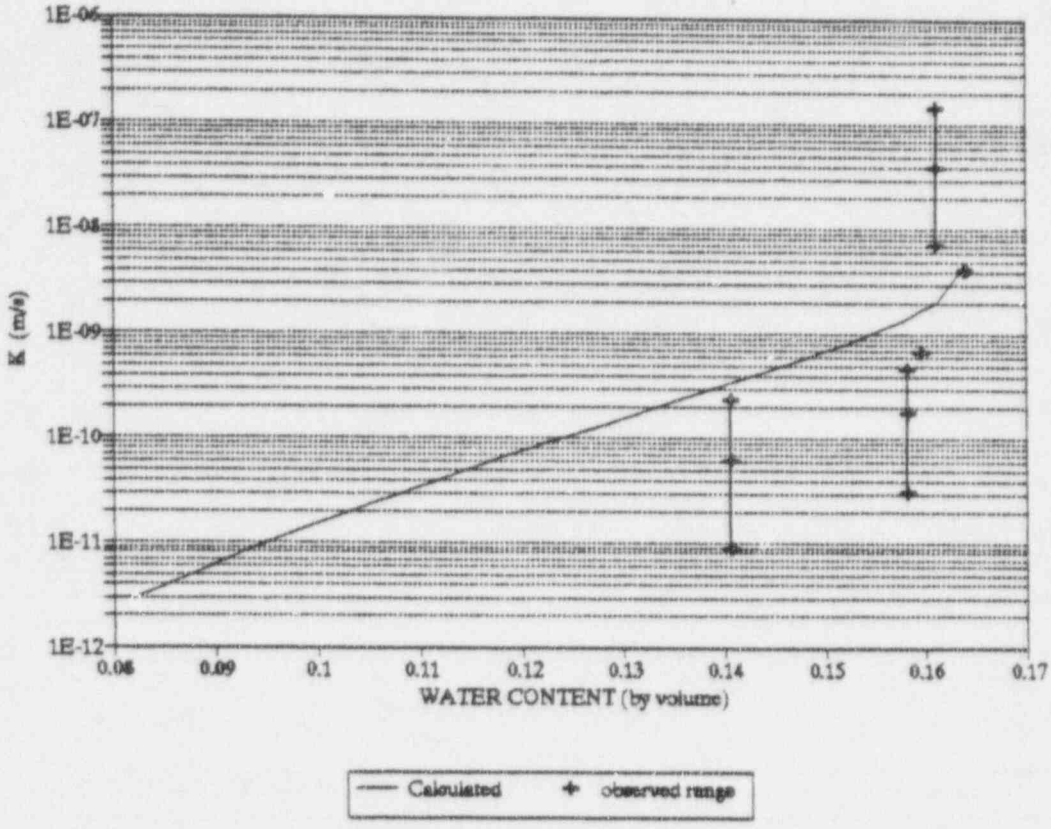

Figure 4.9. Hydraulic conductivity at 20° C: RETC-calculated and the range of conductivity measured at water contents associated with four matric potentials (from Table 4.13).

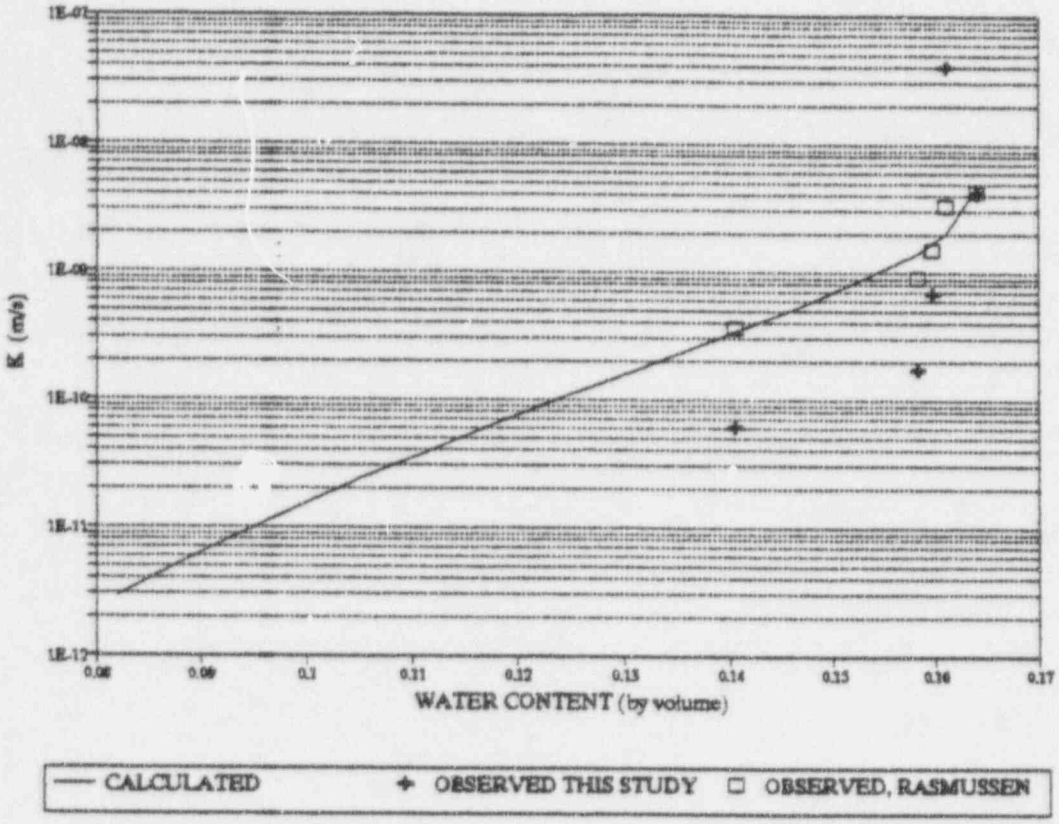

Figure 4.10. Hydraulic conductivity at 20° C: RETC-calculated, observed data from this study, and observed data from Rasmussen et al. (1990).

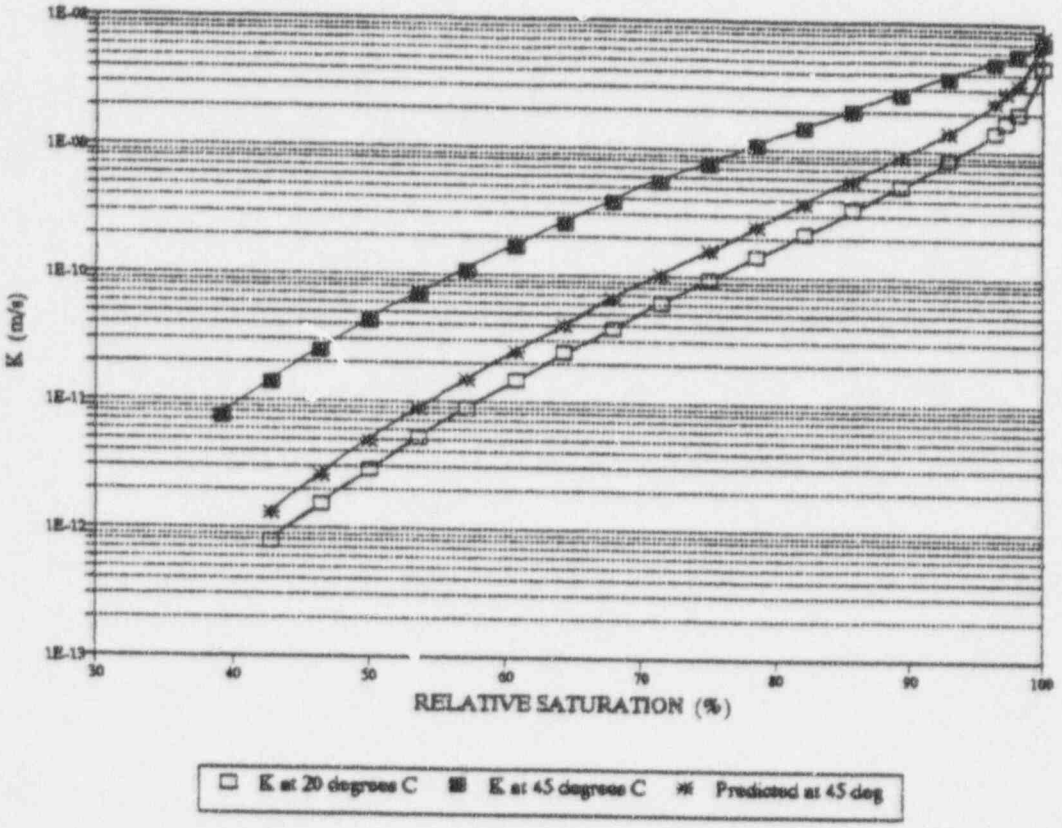

Figure 4.11. RETC-calculated hydraulic conductivity at both 20° and 45° C, and predicted hydraulic conductivity at 45° C.

5. CONCLUSIONS AND RECOMMENDATIONS

The first set of moisture retention curves at 20° C have some notable characteristics. The divergence of the main imbibition curve from the main drying curve at the lowest water contents, distinctly greater than that observed with most granular porous media, may have been caused by a small amount of vapor sorption prior to the onset of fluid flow at 0.5 MPa. The very small amount of clay particles contained in the matrix material results in greatly reduced specific surface and number of available ions. Both of these factors have an influence on vapor adsorption and diffusion (Jackson, 1964; Grismer, 1987). The broader, blunter sigmoidal shape of retention curve sets associated with tuff and other rock samples can be attributed to air entrapment during the wetting process. This is due to the smaller and more variable pore sizes, the increased tortuousity, and the lower permeability of the rock matrix.

The first wetting hysteresis curve indicates a tendency to close with the main drying branch. The occurrence of significant air entrapment is apparent. It is most likely due to high relative saturation, in part preserved by initiating imbibition at 0.5 MPa. The second set of hysteresis scanning curves definitely exhibited the characteristic closed-loop behavior previously observed in granular porous media (Lenhard et al., 1991). While the first scanning curve exhibits the effects of significant air entrapment, the behavior of the second set of curves implies that very little additional air entrapment occurred during the cycle of wetting/drying/wetting. The volume fraction of entrapped air is largely dependent on the degree of saturation of the sample during imbibition, where greater air entrapment occurs at higher levels of relative saturation.

A curve-fitting model and the RETC program for analyzing and predicting hydraulic matrix properties were developed by van Genuchten (1985) and modified by van Genuchten et al. (1991). The model curves depicting moisture retention relationships showed good correlation with measured data for each temperature, indicating satisfactory application of the RETC program to consolidated, low-permeability material such as tuff.

The expected shift of the retention curve toward a higher matric potential was apparent when comparing the fitted 45° C data with the fitted 20° C data. This effect has long been suspected to be caused primarily by the decrease in surface tension of water with increase in temperature (Nimmo, 1983). Physically, this means that, at a higher temperature, the same amount of moisture can be held within the porous media at significantly less matric pressure than it was held at a lower temperature. This definition requires isothermal conditions. While the presence of a thermal gradient demands special attention to the effects of entrapped air (Nimmo, 1983; Hopmans and Dane, 1986), expansion effects of entrapped gases due to thermal changes need not be considered under isothermal conditions. Nevertheless, care was taken (i.e., vacuum-saturation, de-aired solution) to reduce trapped gases which might expand upon release of pressure when samples were removed for weighing.

Confidence in the results of the experiment at 20° C precludes any confidence in the results of the experiment performed at 5° C. Other than nonequilibration, there is no readily apparent cause for the shift of the moisture retention curve toward a lower potential when the shift should have been to the right, toward a higher potential with temperature decrease. Samples were weighed regularly to monitor moisture mass loss, the cessation of which was the signal that samples had reached equilibrium. At 5°, samples required from 5 to 28 days per pressure step to reach equilibrium, often with consistent losses of only a few hundredths of a gram per day. Water vapor flux was not expected to be important at 5° C. Equilibration was expected to take somewhat longer

at the lower temperature, but the much longer time periods may have allowed other factors to affect the process.

The only comparison of hydraulic conductivity curves of interest from this study involve those at 20° and 45° C. The RETC-calculated curves exhibit a shift toward the left with increase in temperature, giving a higher conductivity for a given water content as expected. This effect has been attributed primarily to changes in water viscosity with change in temperature (Constantz, 1982; Hopmans and Dane, 1986). The inverse relationship of viscosity to hydraulic conductivity is commonly employed to predict hydraulic conductivity at new temperatures. As it did in this study, the viscosity ratio method frequently underestimates the changes in K with temperature. Constantz (1982) suggested that the temperature dependence of soil water or saturation extract viscosities may have a greater temperature coefficient than that of free water. Furthermore, at higher temperatures, water vapor may be more important to total isothermal fluid flux in unsaturated media than has previously been allowed.

Primary application of the information generated from this study is to modeling efforts. The relationship of temperature to fluid flow behavior in rock must be incorporated into any comprehensive analysis of unsaturated flow regimes affected by heat sources such as the projected nuclear repository at Yucca Mountain. A realistic assessment of the altered environment requires the identification of truly representative model input parameters and boundary conditions. Accurate hydrologic characterization is difficult to achieve under the best field conditions, and in rock the process is even more challenging. There has been interest shown in experiments where heaters are used to generate thermal gradients under field conditions. Data from this study may offer a useful comparison when such field experiments are realized.

Several recommendations can be made concerning the methodology used for the hydraulic characterization experiments. Equilibration time is a function of the square of the sample height (Klute, 1964). Because of the lengthy equilibration time required for low-permeability material such as tuff, core sample height should be as small as possible without compromising the theory of a representative elementary volume. In addition to the admonition of Klute (1986) to clamp off the outflow tubes of the pressure plate extraction vessel during depressurization to prevent backflow, it is highly recommended that outflow tubes also be removed from contact with any solution.

Rock has a low capacity for thermal conductance. Therefore, samples should be saturated at the temperature of interest, if possible, prior to the onset of the new experiment. Covering samples loosely within the pressure extraction vessel will reduce potential vapor losses during longer equilibration times, especially at higher temperatures where it is more difficult to maintain sufficiently high saturated vapor pressures. Outflow measurements can be difficult to obtain using a permeameter/Tempe cell set-up due to frequent problems of air entrapment within the cell. Air accumulating in the bottom of a Tempe cell may artificially increase the measured outflow of the sample, or it may block outflow. Utilization of wide rubber strips and judicious use of O-ring grease on seals will reduce leaks. The peristaltic pump used to purge the cell and tubing of air must be run at slow speed to prevent back pressure on the sample (Klute, 1986).

6. SUMMARY

Laboratory methods traditionally applied to granular or fine-grained porous media were employed to define matrix hydraulic properties for low-permeability tuff core segments. Moisture content/matric potential relationships, including hysteresis, and measured saturated and unsaturated hydraulic conductivity data were determined at a constant laboratory temperature of 20° C. Hysteretic air entrapment was found to be largely a function of the relative saturation of the media during imbibition, where a higher volume fraction of trapped air occurs when saturation is relatively high.

To investigate the effects of temperature on moisture content/matric potential and moisture content/hydraulic conductivity relationships, additional moisture retention data were obtained at 45° and 5° C. Measured retention and hydraulic conductivity data were applied to the van Genuchten model RETC, which performs curve-fitting and calculation of the flow parameter hydraulic conductivity, K. Although data at 5° proved to be inconclusive, an increase in temperature from 20° to 45° C showed a distinct shift of the moisture characteristic curve toward a higher (less negative) potential at a given water content. Model-calculated hydraulic conductivity curves also showed evidence of the effect of a temperature increase by shifting toward a higher conductivity for a given water content. The inverse relationship between hydraulic conductivity and water viscosity was used to predict K at the higher temperature. It was apparent that, in itself, the temperature-dependent change in the viscosity of water was inadequate to explain the increases of hydraulic conductivity with temperature.

7. REFERENCES

Ashworth, E., and T. Ashworth, 1990, A rapid method for measuring thermal conductivity of rock cores and its preliminary use for finding the thermal resistance of cracks, Rock Mechanics Contributions and Challenges, Hustrulid and Johnson (editors), Balkema, Rotterdam, ISBN 906191 1230.

Bishop, C., 1990, Laboratory determination of hydraulic properties in Eastern Snake River Plain basalts. M.S. Thesis, The University of Arizona, Tucson, Arizona.

Brooks, R.H., and A.T. Corey, 1964, Hydraulic properties of porous media, Colorado State University, Hydrology Paper No. 3, 27 p.

Burdine, N.T., 1953, Relative permeability calculation from size distribution data, Transactions AIME, 198, pp. 71-78.

Campbell, G.S., and G.W. Wee, 1986, Water potential measurement using vapaor equilibration, In A. Klute (ed.) Methods of Soil Analysis, Part I, 2nd ed., Agron. Monogr. 9. ASA and SSSA, Madison, Wisconsin.

Constantz, J., 1982, Temperature dependence of unsaturated hydraulic conductivity of two soils, *Soil Science Society of America Journal*, 46:466-470.

Flint, A., K. Richards, and L. Flint, 199?, Characterization of rock hydrologic properties using model verification, Proceedings from NRC Workshop #5: Flow and Transport Through Unsaturated Fractured Rock.

Gardner, R., 1955, Relation of temperature to moisture tension of soil, *Soil Science*, 79:257-265.

Gardner, R., 1956, Calclulation of capillary conductivity from pressure outflow data, U.S. Salinity Laboratory, Soil and Water Conservation Research Branch, ARS, USDA, Riverside, California.

Grismer, W.R., 1987, Kinetics of water vapor adsorption on soils, *Soil Science*, 143:367-371.

Haridasan, M., and R.D. Jensen, 1972, Effect of temperature on pressure head-water content relationship and conductivity of two soils, Proceedings, *Soil Science Society of America*, 36:703-708.

Hopmans, J.W., and J.H. Dane, 1985, Effect of temperature-dependent hydraulic properties on soil water movement, *Soil Science Society of America Journal*, 49:51-58.

Hopmans, J.W., and J.H. Dane, 1986, Temperature dependence of soil water retention curves, *Soil Science Society of America Journal*, 50:562-567.

Hopmans, J.W., and J.H. Dane, 1986, Temperature dependence of soil hydraulic properties, *Soil Science Society of America Journal*, 50:4-9.

Jackson, R.D., 1964, Water vapor diffusion in relatively dry soil: I. theoretical considerations and sorption experiments, Proceedings, *Soil Science Society of America*, 28:172-176.

Klute, A., 1964, Water diffusivity, In A. Klute (ed.) Methods of Soil Analysis, Part 1, Am. Sc. Agron., *Soil Science Society of America*, Madison, Wisconsin.

Klute, A., 1986, Water Retention: Laboratory methods, In A. Klute (ed.) Methods of Soil Analysis, Part 1, Am. Sc. Agron., *Soil Science Society of America*, Madison, Wisconsin.

Klute, A., and C. Dirksen, 1986, Hydraulic conductivity and diffusivity: laboratory methods, pp. 687-734, In A. Klute (ed.) Methods of Soil Analysis, Part 1, 2nd ed., Agron. Monogr. 9. ASA and SSSA, Madison, Wisconsin.

Kunze, R.J., and D. Kirkham, 1962, Simplified accounting for membrane impedance in capillary conductivity determination, Proceedings, *Soil Science Society of America*, 26:421-426.

Lange, N.A., 1941, (ed.), Handbook of Chemistry and Physics, CRC Press, Boca Raton, 1941.

Lenhard, R., J.C. Parker, and J.J. Kaluarachchi, 1991, Comparing simulated and experimental hysteretic two-phase transient fluid flow phenomena, *Water Resources Research*, 27:2113-2124.

Lindgren, M., and A. Rasmuson, 1990, Two-phase flow simulations in a heated tuff drillcore, Kemakta Consultants Company, Stockholm, Sweden.

Matthews, D.W., 1986, Thermally induced countercurrent flow in unsaturated rock, M.S. Thesis, The University of Arizona, Tucson, Arizona.

Miller, E.E., and D.E. Elrick, 1958, Dynamic determination of capillary conductivity, extended for non-negligible membrane impedence, Proceedings, *Soil Science Society of America*, 22, pp. 483-486.

Mualem, Y., 1976, A new model for predicting the hydraulic conductivity of unsaturated porous media, *Water Resources Research*, 12(3):513-523.

Nimmo, J.R., 1983, The Temperature dependence of soil-moisture characteristics, Ph.D. Dissertation, University of Wisconsin-Madison, Madison, Wisconsin.

Philip, J.R., and D.A. de Vries, 1957, Moisture movement in porous media under temperature gradients, *Transactions*, American Geophysical Union, 38(2):222-232.

Poulovassilis, A., 1970, The effect of the entrapped air on the hysteresis curves of a porous body and on its hydraulic conductivity, *Soil Science*, 109(3):154-162.

Rahi, K.A., 1986, Hydraulic conductivity assessment for a variably saturated rock matrix, M.S. Thesis, The University of Arizona, Tucson, Arizona.

Rasmussen, T.C., D.D. Evans, P.J. Sheets, and J.H. Blanford, 1990, Unsaturated fractured rock characterization methods and data sets at the Apache Leap Tuff Site, Prepared for U.S. Nuclear Regulatory Commission, Dept. of Hydrology and Water Reources, The University of Arizona, Tucson, Arizona, NUREG/CR-5596.

Richards, L.A., 1965, Physical condition of water in soil, In Methods of Soil Analysis, Black, Evans, White, Emsminger and Clark (editors), *Agronomy*, 9:128.

Richards, L.A., 1931, Capillary conduction of liquids through porous mediums, *Physics*, 1, pp. 318-333.

Robinson, R.A., and R.H. Stokes, 1965, Electrolyte Solutions, 2nd ed., Butterworth, London.

Stonestrom, D.A., and J. Rubin, 1989, Water content dependence of trapped air in two soils, *Water Resources Research.*, 25:1947-1958.

Thompson, D., 1990, Field Notebook #107, Core sampling and ID, NRC-04-90-051, Dept. of Hydrology and Water Resources, The University of Arizona, Tucson, Arizona.

Tsang, Y.W., and K. Pruess, 1987, A study of thermally induced convection near a high-level nuclear waste repository in partially saturated fractured tuff, *Water Resources Research*, 23(10):1958-1966.

Valiantzas, J.D., 1990, Analysis of outflow experiments subject to significant plate impedance, *Water Resources Research*, 26(12):2921-2929.

van Genuchten, M.Th., 1980, A closed-form equation for predicting the hydraulic conductivity of unsaturated soils, *Soil Science Society of America Journal*, 44:892-898.

van Genuchten, M.Th., and D.R. Nielsen, 1985, On describing and predicting the hydraulic properties of unsaturated soils, *Annales Geophysicae*, 3(5):615-628.

van Genuchten, M.Th., F.J. Leij, and S.R. Yates, 1991, The RETC code for quantifying the hydraulic functions of unsaturated soils, U.S. Salinity Laboratory, USDA-ARS, Riverside, California.

Wang, J.S.Y., C.F. Tsang, N.G.W. Cook, and P.A. Witherspoon, 1981, A study of regional temperature and thermohydrologic effects of an underground repository for nuclear wastes in hard rock, *Journal of Geophysical Research*, 86:3759-3770.

Wilkinson, G.E., and A. Klute, 1962, The temperature effect on the equilibrium energy status of water held by porous media, Proceedings, *Soil Science Society of America*, 26:326-329.

APPENDIX A

LABORATORY-MEASURED MOISTURE RETENTION AND HYDRAULIC CONDUCTIVITY DATA FOR APACHE LEAP TUFF

Table A.1. Moisture Retention Data for Apache Leap Tuff at 20° C.

Desorption:

Sample #	Matric Potential (MPa)								
	.010	.025	.050	.10	.30	.50	2.73	14.24	23.57
0701	0.1555	0.1547	0.1503	0.1361	0.1141	0.0919	0.0567	0.0270	0.0207
0702	0.1679	0.1673	0.1637	0.1507	0.1151	0.0911	0.0584	0.0294	0.0224
0703	0.1430	0.1423	0.1426	0.1341	0.1041	0.0892	0.0613	0.0311	0.0237
0704	0.1544	0.1536	0.1494	0.1299	0.0944	0.0812	0.0614	0.0287	0.0222
0705	0.1569	0.1560	0.1544	0.1455	0.1111	0.0954	0.0578	0.0294	0.0225
0706	0.1676	0.1665	0.1591	0.1425	0.1040	0.0833	0.0571	0.0281	0.0217
0707	0.1527	0.1523	0.1513	0.1409	0.1153	0.0953	0.0607	0.0301	0.0230
0708	0.1497	0.1488	0.1453	0.1208	0.0905	0.0777	0.0626	0.0314	0.0239
0709	0.1639	0.1623	0.1597	0.1495	0.1209	0.0970	0.0565	0.0285	0.0214
0710	0.1594	0.1588	0.1548	0.1391	0.1118	0.0913	0.0553	0.0286	0.0225
0711	0.1607	0.1586	0.1551	0.1370	0.1253	0.0884	0.0608	0.0345	0.0251
0712	0.1625	0.1599	0.1542	0.1424	0.1114	0.0795	0.0540	0.0294	0.0213
0713	0.1688	0.1667	0.1627	0.1433	0.1283	0.0855	0.0544	0.0299	0.0225
0714	0.1617	0.1600	0.1556	0.1434	0.1202	0.0879	0.0553	0.0300	0.0220
0715	0.1672	0.1658	0.1620	0.1423	0.1103	0.0829	0.0604	0.0333	0.0244
0716	0.1740	0.1695	0.1623	0.1394	0.1148	0.0806	0.0570	0.0306	0.0224
0717	0.1630	0.1606	0.1532	0.1371	0.1047	0.0759	0.0543	0.0292	0.0216
0718	0.1618	0.1606	0.1554	0.1425	0.1148	0.0813	0.0597	0.0325	0.0220
0719	0.1582	0.1559	0.1473	0.1331	0.1059	0.0793	0.0557	0.0316	0.0230
0720	0.1740	0.1722	0.1660	0.1429	0.1071	0.0813	0.0576	0.0309	0.0220

Table A.1. (Continued)

Absorption:

SAMPLE#	Matric Potential (MPa)							
	.010	.025	.050	.10	.30	.50	2.73	14.24
0701	-	-	-	-	-	0.0506	0.0249	0.0221
0702	-	-	-	-	-	0.0547	0.0272	0.0242
0703	-	-	-	-	-	0.0561	0.0282	0.0250
0704	-	-	-	-	-	0.0560	0.0266	0.0234
0705	-	-	-	-	-	0.0622	0.0278	0.0245
0706	-	-	-	-	-	0.0620	0.0265	0.0237
0707	-	-	-	-	-	0.0581	0.0283	0.0250
0708	-	-	-	-	-	0.0555	0.0293	0.0261
0709	-	-	-	-	-	0.0574	0.0270	0.0236
0710	-	-	-	-	-	0.0529	0.0268	0.0243
0711	0.1327	0.1276	0.1174	0.0996	0.0785	0.0664	0.0310	0.0269
0712	0.1345	0.1279	0.1111	0.0878	0.0683	0.0573	0.0264	0.0233
0713	0.1419	0.1323	0.1153	0.0940	0.0713	0.0621	0.0280	0.0245
0714	0.1291	0.1233	0.1101	0.0908	0.0720	0.0609	0.0274	0.0240
0715	0.1365	0.1308	0.1198	0.0996	0.0806	0.0720	0.0303	0.0265
0716	0.1455	0.1371	0.1198	0.1003	0.0855	0.0707	0.0278	0.0245
0717	0.1282	0.1227	0.1060	0.0858	0.0711	0.0607	0.0268	0.0236
0718	0.1329	0.1274	0.1139	0.0908	0.0729	0.0627	0.0285	0.0250
0719	0.1309	0.1255	0.1145	0.0943	0.0747	0.0660	0.0288	0.0251
0720	0.1430	0.1366	0.1228	0.1005	0.0758	0.0641	0.0284	0.0248

Table A.2. Relative Saturation Data for Apache Leap Tuff at 20° C.

Desorption:

Sample #	Matric Potential (MPa)								
	.010	.025	.050	.10	.30	.50	2.73	14.24	23.57
0701	94.41	93.93	91.26	82.64	69.28	55.80	34.43	16.39	12.57
0702	96.66	96.32	94.24	86.76	66.26	52.45	33.62	16.93	12.90
0703	96.56	96.08	96.29	90.55	70.29	60.23	41.39	21.00	16.00
0704	96.26	95.76	93.14	80.99	58.85	50.62	38.28	17.89	13.83
0705	96.67	96.12	95.13	89.65	68.45	58.78	35.61	18.11	13.86
0706	94.21	93.59	89.43	80.10	58.46	46.82	32.10	15.80	12.20
0707	97.08	96.82	96.19	89.57	73.30	60.58	38.59	19.14	14.62
0708	97.14	96.56	94.29	78.39	58.73	50.42	40.62	20.38	15.51
0709	97.50	96.55	95.00	88.94	71.92	57.70	33.61	16.95	12.73
0710	95.45	95.09	92.69	83.29	66.95	54.67	33.11	17.13	13.47
0711	98.47	97.18	95.04	83.95	76.78	54.17	37.25	21.14	15.38
0712	97.77	96.21	92.78	85.68	67.03	47.83	32.49	17.69	12.82
0713	96.90	95.69	93.40	82.26	73.65	49.08	31.23	17.16	12.92
0714	97.59	96.56	93.90	86.54	72.54	53.05	33.37	18.11	13.28
0715	98.01	97.19	94.96	83.41	64.65	48.59	35.40	19.52	14.30
0716	97.81	95.28	91.23	78.36	64.53	45.31	32.04	17.20	12.59
0717	98.19	96.75	92.29	82.59	63.07	45.72	32.71	17.59	13.01
0718	98.54	97.81	94.64	86.78	69.91	49.51	36.36	19.79	14.01
0719	98.02	96.59	91.26	82.47	65.61	49.13	34.51	19.58	14.25
0720	98.36	97.34	93.84	80.78	60.54	45.96	32.56	17.47	12.44

Table A.2. (Continued)

Absorption:

Sample #	Matric Potential (MPa)							
	.010	.025	.050	.10	.30	.50	2.73	14.24
0701	-	-	-	-	-	30.72	15.12	13.42
0702	-	-	-	-	-	31.49	15.66	13.93
0703	-	-	-	-	-	37.88	19.04	16.88
0704	-	-	-	-	-	34.91	16.58	14.59
0705	-	-	-	-	-	38.32	17.13	15.10
0706	-	-	-	-	-	34.85	14.90	13.32
0707	-	-	-	-	-	36.94	17.99	15.89
0708	-	-	-	-	-	36.02	19.01	16.94
0709	-	-	-	-	-	34.15	16.06	14.04
0710	-	-	-	-	-	31.68	16.05	14.55
0711	80.57	77.47	71.28	60.47	47.66	40.69	19.00	16.48
0712	77.43	73.63	63.96	50.55	39.32	32.99	15.20	14.02
0713	95.81	89.33	77.85	63.47	48.14	41.93	18.91	14.06
0714	80.49	76.87	68.64	56.61	44.89	37.97	17.08	14.48
0715	84.10	80.59	73.81	61.37	49.66	44.36	18.67	15.53
0716	81.79	77.07	67.34	56.38	48.06	39.74	15.63	13.77
0717	81.50	78.00	67.39	54.55	45.20	38.59	17.04	14.22
0718	86.24	82.67	73.91	58.92	47.31	40.69	18.49	15.23
0719	77.87	74.66	68.11	56.10	44.44	39.26	17.13	15.55
0720	85.63	81.80	73.53	60.18	45.39	38.38	17.01	14.02

Table A.3. Hysteresis Data for ALT at 20° C, water content, sorbing from 0.5 MPa.

Sample #	Matric Potential (MPa)					
	0.010	.025	.050	.10	.30	.50
0721	0.1360	0.1307	0.1114	0.0987	0.0855	0.0785
0722	0.1271	0.1191	0.1021	0.0919	0.0829	0.0769
0723	0.1328	0.1292	0.1188	0.1096	0.1001	0.0958
0724	0.1261	0.1226	0.1117	0.1037	0.1048	0.0852
0725	0.1250	0.1074	0.1075	0.1000	0.0880	0.0753
0726	0.1365	0.1294	0.1101	0.1007	0.0895	0.0876
0727	0.1311	0.1283	0.1182	0.1089	0.0962	0.0847
0728	0.1366	0.1334	0.1241	0.1132	0.1011	0.0914
0729	0.1308	0.1249	0.1047	0.0939	0.0858	0.0838
0730	0.1351	0.1294	0.1112	0.0967	0.0836	0.0792

Table A.4. Hysteresis Data for ALT at 20° C, relative saturation, sorbing from 0.5 MPa.

Sample #	Matric Potential (MPa)					
	0.010	0.025	.050	0.10	0.30	0.50
0721	93.21	89.58	76.35	67.65	58.60	53.80
0722	91.18	85.44	73.24	65.93	59.47	55.16
0723	91.40	88.92	81.76	75.43	68.89	65.93
0724	94.95	92.32	84.11	78.09	78.92	64.16
0725	92.94	79.85	79.93	74.35	65.43	55.99
0726	94.27	89.36	76.04	69.54	61.81	60.50
0727	92.78	90.80	83.65	77.07	68.08	59.94
0728	92.74	90.56	84.25	76.85	68.64	62.05
0729	96.46	92.11	77.21	69.25	63.27	61.80
0730	87.78	84.08	72.25	62.83	54.32	51.46

Table A.5. Hysteresis Loop Data at 20° C, water content, desorbing to/absorbing from 0.5 MPa.

Desorbing:

	Matric Potential (MPa)					
Sample #	0.01	0.025	0.05	0.10	0.30	0.50
0711	-	0.1261	0.1247	0.1131	0.0830	0.0723
0712	-	0.1254	0.1209	0.1064	0.0799	0.0684
0713	-	0.1300	0.1239	0.1063	0.0806	0.0671
0714	-	0.1202	0.1132	0.0944	0.0733	0.0642
0715	-	0.1278	0.1226	0.1029	0.0782	0.0692
0716	-	0.1335	0.1270	0.1100	0.0818	0.0699
0717	-	0.1190	0.1146	0.0998	0.0741	0.0639
0718	-	0.1234	0.1198	0.1041	0.0783	0.0677
0719	-	0.1223	0.1186	0.1048	0.0820	0.0698
0720	-	0.1334	0.1297	0.1146	0.0865	0.0726

Absorbing:

	Matric Potential (MPa)					
Sample #	0.01	0.025	0.05	0.10	0.30	0.50
0711	0.1380	0.1306	0.1137	0.1021	0.0780	-
0712	0.1375	0.1276	0.1055	0.0973	0.0729	-
0713	0.1458	0.1312	0.1105	0.1012	0.0722	-
0714	0.1335	0.1232	0.1029	0.0954	0.0694	-
0715	0.1423	0.1345	0.1166	0.1043	0.0753	-
0716	0.1490	0.1355	0.1156	0.1055	0.0753	-
0717	0.1320	0.1207	0.1039	0.0967	0.0697	-
0718	0.1372	0.1296	0.1113	0.1012	0.0738	-
0719	0.1367	0.1270	0.1121	0.0988	0.0748	-
0720	0.1469	0.1382	0.1201	0.1045	0.0779	-

Table A.6. Hysteresis Loop Data at 20° C, relative saturation, desorbing to/absorbing from 0.5 MPa.

Desorbing:

	Matric Potential (MPa)					
Sample	.010	.025	.050	.100	.300	.500
0711	-	77.27	76.41	69.30	50.86	44.30
0712	-	75.45	72.74	64.02	48.07	41.16
0713	-	74.63	71.13	61.02	46.27	38.52
0714	-	72.54	68.32	56.97	44.24	38.74
0715	-	74.91	71.86	60.32	45.84	40.56
0716	-	75.04	71.39	61.83	45.98	39.29
0717	-	71.69	69.04	60.12	44.64	38.49
0718	-	75.15	72.96	63.40	47.69	41.23
0719	-	75.77	73.48	64.93	50.81	43.25
0720	-	75.41	73.32	64.78	48.90	41.04

Absorbing:

	Matric Potential (MPa)					
Sample	.010	.025	.050	.100	.300	.500
0711	84.56	80.02	69.67	62.56	47.79	-
0712	82.73	76.77	63.48	58.54	43.86	-
0713	83.70	75.32	63.43	58.09	41.45	-
0714	80.57	74.35	62.10	57.57	41.88	-
0715	83.41	78.84	68.35	61.14	44.14	-
0716	83.75	76.17	64.98	59.30	42.33	-
0717	79.52	72.71	62.59	58.25	41.99	-
0718	83.56	78.93	67.78	61.63	44.95	-
0719	84.70	78.69	69.45	61.21	46.34	-
0720	83.04	78.12	67.89	59.07	44.04	-

Table A.7. Moisture Retention Data for ALT at 45° C, water content (ccm/ccm).

Desorbing:

	Matric Potential (MPa)						
Sample	0 (sat)	0.01	0.025	0.05	0.10	0.30	0.50
0701	0.1845	0.1600	0.1604	0.1499	0.1139	0.0628	0.0634
0702	0.1824	0.1687	0.1680	0.1589	0.1314	0.0693	0.0697
0703	0.1613	0.1502	0.1505	0.1445	0.1118	0.0742	0.0719
0704	0.1777	0.1625	0.1625	0.1511	0.1178	0.0711	0.0687
0705	0.1716	0.1603	0.1575	0.1464	0.1166	0.0719	0.0685
0706	0.1832	0.1633	0.1598	0.1470	0.1073	0.0681	0.0662
0707	0.1699	0.1535	0.1512	0.1429	0.1128	0.0691	0.0669
0708	0.1602	0.1485	0.1447	0.1429	0.1083	0.0668	0.0664
0709	0.1713	0.1607	0.1580	0.1486	0.1162	0.0710	0.0682
0710	0.1818	0.1656	0.1626	0.1487	0.1084	0.0619	0.0622
0711	0.1665	0.1579	0.1561	0.1450	0.1246	0.0741	0.0714
0712	0.1752	0.1648	0.1651	0.1547	0.1288	0.0720	0.0687
0713	0.1812	0.1684	0.1642	0.1521	0.1210	0.0721	0.0683
0714	0.1722	0.1627	0.1633	0.1487	0.1194	0.0711	0.0679
0715	0.1757	0.1670	0.1659	0.1550	0.1256	0.0744	0.0710
0716	0.1837	0.1679	0.1643	0.1538	0.1335	0.0700	0.0681
0717	0.1716	0.1602	0.1557	0.1451	0.1229	0.0663	0.0646
0718	0.1711	0.1606	0.1591	0.1501	0.1295	0.0703	0.0692
0719	0.1662	0.1550	0.1545	0.1454	0.1263	0.0740	0.0710
0720	0.1794	0.1672	0.1515	0.1567	0.1456	0.0748	0.0727

Table A.8. Moisture Retention Data for ALT at 45° C, relative saturation (%).

Desorbing:

	Matric Potential (MPa)					
Sample	0.01	0.025	0.05	0.10	0.30	0.50
0701	91.77	92.02	86.02	65.37	36.05	36.37
0702	96.78	96.36	91.17	75.36	39.73	39.98
0703	86.15	86.32	82.89	64.15	42.57	41.24
0704	93.21	93.21	86.68	67.59	40.82	39.41
0705	91.97	90.39	83.97	66.90	41.24	39.32
0706	93.68	91.67	84.31	61.56	39.06	37.97
0707	88.08	86.74	81.97	64.74	39.65	38.39
0708	85.19	83.01	81.96	62.12	38.32	38.08
0709	92.18	90.67	85.23	66.66	40.73	39.15
0710	95.02	93.31	85.33	62.18	35.51	35.68
0711	90.60	89.55	83.18	71.48	42.52	40.98
0712	94.55	94.71	88.77	73.90	41.30	39.40
0713	96.62	94.20	87.27	69.43	41.37	39.19
0714	93.36	93.68	85.32	68.52	40.82	38.93
0715	95.82	95.16	88.93	72.05	42.70	40.74
0716	96.35	94.26	88.24	76.58	40.18	39.06
0717	91.93	89.31	83.27	70.54	38.04	37.06
0718	92.17	91.29	86.11	74.31	40.34	39.71
0719	88.92	88.62	83.42	72.48	42.43	40.75
0720	95.93	86.95	89.89	83.52	42.94	41.72

Table A.9. Moisture Retention Data for ALT at 5° C, water content.

Desorbing:

	Matric Potential (MPa)						
Sample	0 (sat)	0.01	0.025	0.05	0.10	0.30	0.50
0701	0.1839	0.1836	0.1777	0.1654	0.1304	0.0818	0.0734
0702	0.1818	0.1812	0.1783	0.1725	0.1377	0.0881	0.0777
0703	0.1595	0.1592	0.1575	0.1532	0.1154	0.0866	0.0791
0704	0.1766	0.1749	0.1721	0.1644	0.1189	0.0850	0.0769
0705	0.1705	0.1704	0.1664	0.1608	0.1248	0.0883	0.0782
0706	0.1821	0.1794	0.1734	0.1618	0.1201	0.0819	0.0741
0707	0.1686	0.1662	0.1636	0.1579	0.1203	0.0853	0.0764
0708	0.1610	0.1541	0.1509	0.1436	0.1104	0.0778	0.0712
0709	0.1735	0.1735	0.1698	0.1610	0.1211	0.0858	0.0778
0710	0.1815	0.1781	0.1735	0.1631	0.1150	0.0814	0.0731
0711	0.1684	0.1683	0.1663	0.1600	0.1189	0.0876	0.0792
0712	0.1748	0.1744	0.1717	0.1624	0.1198	0.0882	0.0776
0713	0.1819	0.1771	0.1707	0.1607	0.1228	0.0857	0.0764
0714	0.1737	0.1737	0.1715	0.1645	0.1314	0.0852	0.0764
0715	0.1769	0.1739	0.1722	0.1648	0.1215	0.0884	0.0805
0716	0.1842	0.1832	0.1771	0.1649	0.1276	0.0864	0.0788
0717	0.1740	0.1737	0.1706	0.1612	0.1281	0.0820	0.0737
0718	0.1749	0.1738	0.1715	0.1640	0.1255	0.0864	0.0789
0719	0.1683	0.1683	0.1650	0.1560	0.1186	0.0875	0.0785
0720	0.1800	0.1774	0.1597	0.1636	0.1234	0.0888	0.0798

Table A.10. Moisture Retention Data for ALT at 5° C, relative saturation.

Desorbing:

	Matric Potential (MPa)					
Sample	0.01	0.025	0.05	0.10	0.30	0.50
0701	99.82	96.63	89.94	70.93	44.48	39.91
0702	99.67	98.08	94.90	75.76	48.44	42.72
0703	99.82	98.74	96.02	72.31	54.30	49.60
0704	99.02	97.48	93.12	67.36	48.14	43.53
0705	99.91	97.55	94.26	73.18	51.77	45.87
0706	98.56	95.23	88.88	65.97	44.96	40.67
0707	98.54	97.00	93.66	71.32	50.60	45.29
0708	95.76	93.77	89.18	68.60	48.35	44.20
0709	99.99	97.83	92.75	69.79	49.41	44.84
0710	98.11	95.58	89.87	63.37	44.86	40.29
0711	99.99	98.75	95.03	70.63	52.02	47.06
0712	99.75	98.18	92.87	68.50	50.46	44.37
0713	97.38	93.83	88.36	67.51	47.10	42.00
0714	99.99	98.68	94.69	75.64	49.02	43.97
0715	98.30	97.34	93.19	68.71	49.99	45.51
0716	99.45	96.14	89.51	69.26	46.90	42.76
0717	99.82	98.04	92.62	73.59	47.12	42.34
0718	99.35	98.01	93.77	71.74	49.40	45.07
0719	99.98	98.02	92.69	70.50	51.99	46.66
0720	98.57	88.71	90.90	68.58	49.32	44.31

Table A.11. Saturated Intrinsic Permeability (m sq).

Sample #	k
0732	3.05E-16
0735	3.42E-16
0736	4.18E-16
0737	4.42E-16
0739	6.02E-16
0740	4.63E-16
0741	1.39E-14
0742	3.74E-16
0744	3.28E-16
0745	8.76E-16

Table A.12. Intrinsic Permeability Data for ALT at 20° C.

	Matric Potential (MPa)			
Sample	0.01	0.025	0.05	0.10
0701	7.33E-16	6.99E-17	4.73E-17	2.44E-17
0702				
0703	1.53E-14			1.13E-17
0704				4.44E-18
0705				1.30E-17
0706			3.22E-18	
0707	1.12E-15			2.44E-18
0708				2.71E-18
0709			2.76E-18	
0710				
0711				9.19E-19
0712				3.12E-18
0713		6.90E-17		
0714				
0715	1.21E-15			
0716	2.40E-15			4.62E-18
0717				1.21E-18
0718				3.20E-18
0719				6.28E-18
0720				4.10E-18

APPENDIX B

THERMAL CONDUCTIVITY MEASUREMENTS FOR APACHE LEAP TUFF: LABORATORY RESULTS AND PROCEDURES

Because thermal gradients can substantially affect the movement of water as liquid and vapor in the subsurface, characterization of the moisture-dependent thermal properties of the rock matrix is important for modeling thermal effects on fluid and solute transport. This section includes statistical summaries of the laboratory-derived thermal conductivities corresponding to samples which were used for other experiments included in this report.

To estimate thermal properties of the rock matrix, modifications were made to a new method (Ashworth, 1990) where core segments were "sandwiched" between sets of copper disks with thermistors and heat exchangers, as shown in Figure B.1. The "heat flux meter" of copper/nylon/copper disks, positioned on the top surface of the core, was the mechanism by which the amount of heat flux entering the segment could be measured. A thermal gradient was imposed vertically through the sample, and the steady-state temperature of the core was evaluated with the thermistor/copper disk at the core's lower surface. By using materials of known thermal conductivity and low thermal resistivity where appropriate, Fourier's Law can be used to calculate thermal conductivity for core samples of known length.

Table B.1 summarizes the laboratory thermal conductivities for given mean water contents at oven dry, saturation, and two intermediate steps. These mean K_T values are plotted in Figure B.2. Table B.2 presents data for individual segments.

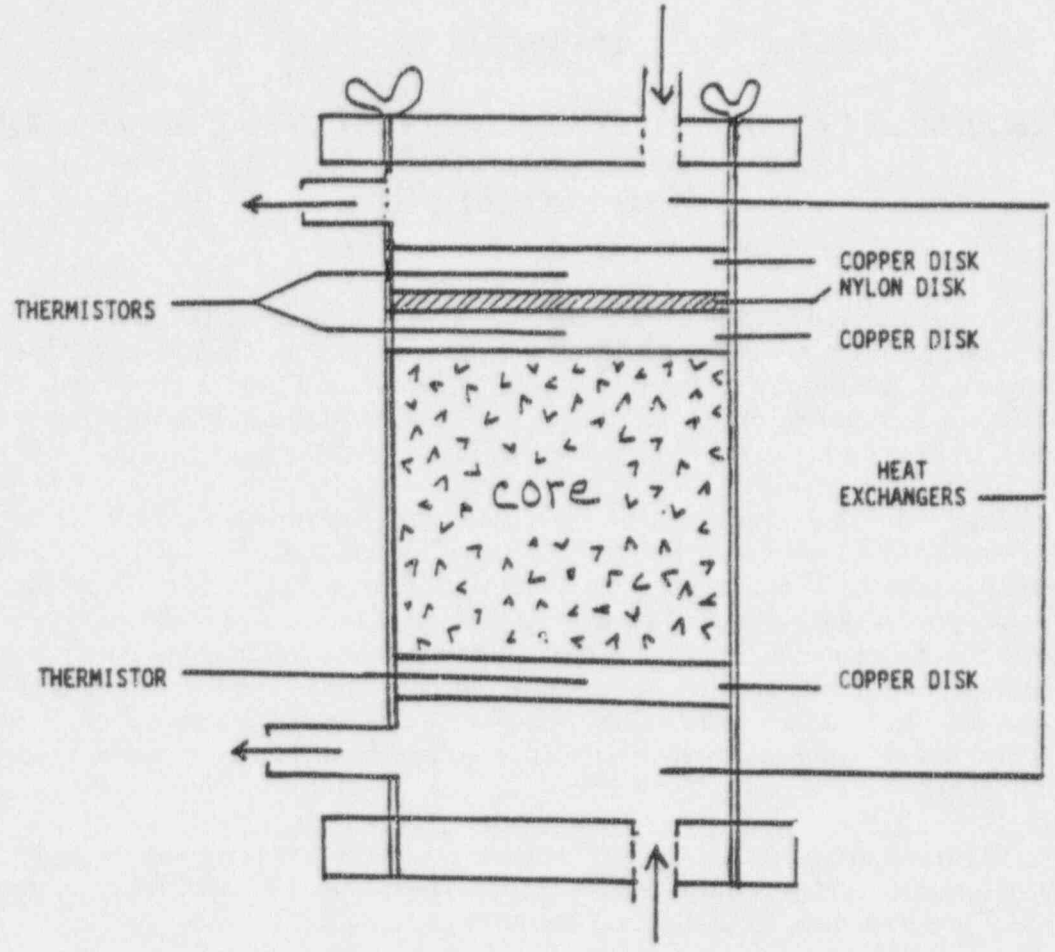

Figure B.1. Apparatus for measuring thermal conductivity of a single consolidated sample.

Table B.1. Statistical Summary of Thermal Conductivity for Variably Saturated Apache Leap Tuff, J/sm° C.

	Water content (mean, % by volume)			
	15.02 (sat)	9.22	2.67	0
# repetitions	10	9	3	9
Mean	1.899	1.574	1.382	1.305
Coef.var.	0.0134	0.0193	0.0299	0.0282
Minimum	1.786	1.47	1.341	1.168
Median	1.864	1.54	1.341	1.289
Maximum	2.027	1.703	1.465	1.533

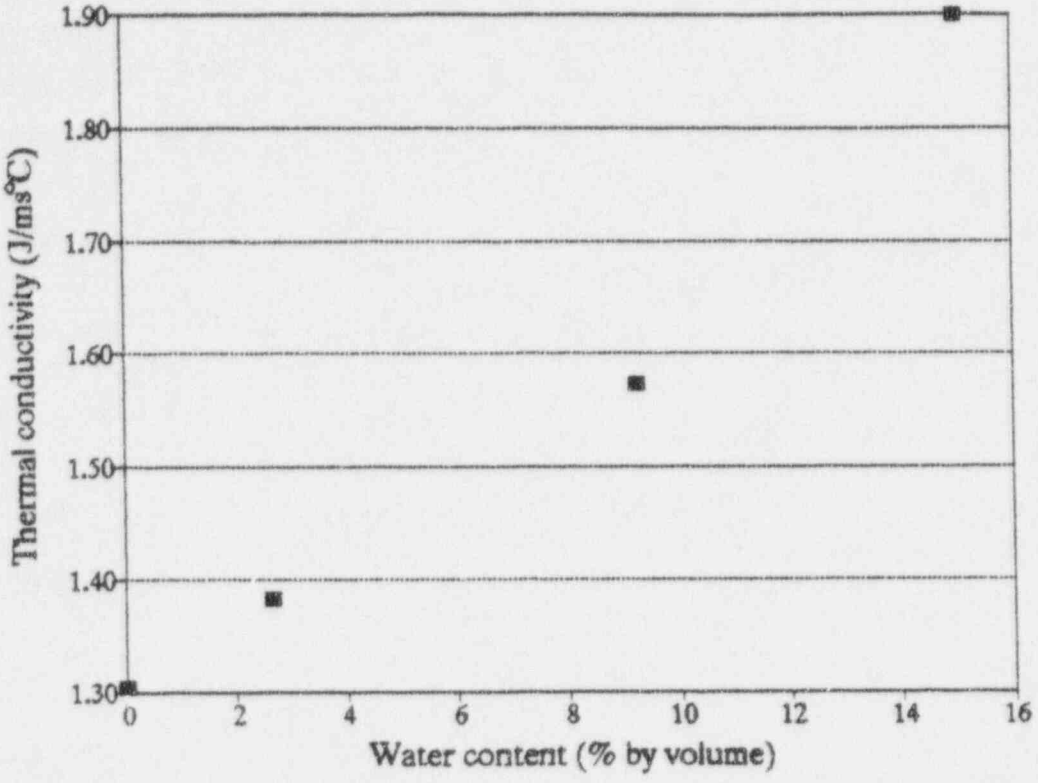

Figure B.2. Graph of thermal conductivity for variably saturated Apache Leap Tuff.

Table B.2. Thermal Conductivity Data for Variably Saturated Apache Leap Tuff, J/sm° C.

	Water content (mean, % by volume)			
Sample #	15.02 (sat)	9.22	2.67	0
0721	1.921	1.703		1.302
0722	2.027	1.676	1.465	1.389
0723	1.947	1.470		1.168
0724	1.827	1.507		1.356
0725	1.855	1.525		1.533
0726	2.015	1.693	1.341	1.252
0727	1.864	1.511	1.341	1.289
0728	1.914	1.565		1.197
0729	1.830	1.511		1.258
0730	1.786			

NRC FORM 335 (2-89) NRCM 1102, 3201, 3202

U.S. NUCLEAR REGULATORY COMMISSION

BIBLIOGRAPHIC DATA SHEET

(See instructions on the reverse)

1. REPORT NUMBER (Assigned by NRC, Add Vol., Supp., Rev., and Addendum Numbers, if any.)
NUREG/CR-6458

2. TITLE AND SUBTITLE
Moisture Characteristic Curves for Apache Leap Tuff: Temperature Effects and Hysteresis

3. DATE REPORT PUBLISHED
MONTH: September
YEAR: 1996

4. FIN OR GRANT NUMBER
L1282

5. AUTHOR(S)
C. R. Rhodes, L. G. Wilson, T. C. Rasmussen, R. L. Bassett

6. TYPE OF REPORT
Technical

7. PERIOD COVERED (Inclusive Dates)

8. PERFORMING ORGANIZATION – NAME AND ADDRESS (If NRC, provide Division, Office or Region, U.S. Nuclear Regulatory Commission, and mailing address; if contractor, provide name and mailing address.)
Department of Hydrology and Water Resources
The University of Arizona
Tucson, AZ 85721

9. SPONSORING ORGANIZATION – NAME AND ADDRESS (If NRC, type "Same as above"; if contractor, provide NRC Division, Office or Region, U.S. Nuclear Regulatory Commission, and mailing address.)
Division of Regulatory Applications
Office of Nuclear Regulatory Research
U.S. Nuclear Regulatory Commission
Washington, DC 20555-0001

10. SUPPLEMENTARY NOTES
T. Nicholson, NRC Project Manager

11. ABSTRACT (200 words or less)

Laboratory methods were use to define matrix hydraulic properties for low-permeability Apache Leap Tuff core segments. Moisture content/matric potential relationships, including hysteresis, and measured hydraulic conductivity data were determined at a constant laboratory temperature of 20 C. To investigate the effects of temperature on those relationships, additional retention data were obtained at 5 C and 45 C. Measured retention data at all temperatures were applied to the van Genuchten model RETC, which performs curve-fitting and calculation of the flow parameter hydraulic conductivity. Although data at 5 C proved to be inconclusive, increasing the temperature from 20 to 45 C produced a shift of the moisture characteristic curve toward a higher potential for a given water saturation. Model calculated hydraulic conductivity also increased as temperature increased, with respect to water saturation. The temperature-dependent change in the viscosity of water proved inadequate to explain the increases of hydraulic conductivity with temperature.

12. KEY WORDS/DESCRIPTORS (List words or phrases that will assist researchers in locating the report.)
unsaturated flow, tuff, Apache Leap, radioactive waste, moisture characteristic curves

13. AVAILABILITY STATEMENT
Unlimited

14. SECURITY CLASSIFICATION
(This Page) Unclassified
(This Report) Unclassified

15. NUMBER OF PAGES

16. PRICE

NRC FORM 335 (2-89)

Federal Recycling Program

UNITED STATES
NUCLEAR REGULATORY COMMISSION
WASHINGTON, DC 20555-0001

OFFICIAL BUSINESS
PENALTY FOR PRIVATE USE, $300

SPECIAL STANDARD MAIL
POSTAGE AND FEES PAID
USNRC
PERMIT NO. G-67

12^555139531 1 1AN1RW1WH
US NRC-OADM
DIV FOIA & PUBLICATIONS SVCS
TPS-PDR-NUREG
2WFN-6E7
WASHINGTON DC 20555